Research Article

Khalid K. Ali*, Tasneem Adel, Mansour N. Abd El-Salam, Mohamed S. Mohamed, and Mohamed A. Shaalan

Optical soliton solutions, bifurcation analysis, chaotic behaviors of nonlinear Schrödinger equation and modulation instability in optical fiber

https://doi.org/10.1515/phys-2025-0164
received November 29, 2024; accepted April 15, 2025

Abstract: In this study, we use the powerful and strong method to obtain a solution of the Sasa–Satsuma equation as $(\mathcal{H} + \frac{\mathcal{G}'}{\mathcal{G}^2})$-expansion method. This method plays a considerable role in solving nonlinear partial differential equations (NPDEs). We investigate the modulation instability in higher-order NPDEs. Modulation instability is a phenomenon observed in certain types of nonlinear systems, such as optical fiber or plasma waves. Modulation instability is a key process in generating optical solitons, rogue waves, and interest in various fields such as nonlinear optics and plasma physics. Using a linearizing technique, we establish the modulation instability and show the influence of a higher nonlinear component in modulation instability. We examine the bifurcation analysis of the Sasa–Satsuma equation. The time histories and Poincare mapping are used to scrutinize the chaotic behaviors of the dynamical system of the Sasa–Satsuma equation excited by a parametric excitation force. To control the vibrating system, use proportional feedback control (P-Controller). Two-dimensional and three-dimensional figures are presented for singular, dark, and bright optical soliton solutions related to optical fiber. These graphs are very important and useful in describing the behavior of solutions.

*** Corresponding author: Khalid K. Ali,** Mathematics Department, Faculty of Science, Al-Azhar University, Nasr-City, Cairo, Egypt, e-mail: khalidkaram2012@azhar.edu.eg
Tasneem Adel: Al-Obour Higher Institute for Engineering and Technology, Al Obour City, Egypt, e-mail: Tasneem.adel.un@gmail.com
Mansour N. Abd El-Salam: Higher Technological Institute, Tenth of Ramadan City, Egypt, e-mail: mansour.naserallah@yahoo.com
Mohamed S. Mohamed: Department of Mathematics, College of Science, Taif University, P.O. Box 11099, Taif, 21944, Saudi Arabia, e-mail: m.saaad@tu.edu.sa
Mohamed A. Shaalan: Higher Technological Institute, Tenth of Ramadan City, Egypt, e-mail: abozeid87@yahoo.com

Keywords: Sasa–Satsuma equation, $(\mathcal{H} + \frac{\mathcal{G}'}{\mathcal{G}^2})$-expansion method, nonlinear optical system, qualitative analysis, dynamical system, P-controller

1 Introduction

Nonlinear partial differential equations (NPDEs) are a type of mathematical equation. NPDEs are more complex and challenging to solve. They arise in various fields, including physics, engineering, and finance, to model diverse phenomena like fluid dynamics, wave propagation, and phase transitions. Solving NPDEs often requires advanced techniques such as numerical methods, perturbation methods, or transforming them into equivalent integral equations. The solutions of NPDEs can lead to fascinating and intricate patterns, making them an essential tool in understanding many real-world applications [1–9].

The soliton solutions of NPDEs such as Schrödinger equation [2], Akshmanan–Prosezain–Daniel equation [10], Navier–Stokes equation [11], Korteweg–De Vries equation [12], Burgers' equation [13], higher-order nonlinear Schrödinger equation [14], Biswas–Arshed equation [15], Kundu–Eckhaus equation [16], and Davey–Stewartson–Kadomtsev–Petviashvili equation [17] are studied by different techniques.

There are several methods to solve the Sasa–Satsuma equation, such as Darboux transformation [18], Sinh–Gordon expansion method [19], modified Kudryashov method [20], F-expansion method [21], modified simple equation method [22], improved modified extended tanh scheme [23], new version of Kudryashov and exponential method [24], trial equation method [25], ∂-dressing method[26], ∂ method [27], extend trial equation method, and generalized Kudryashov method [28].

In this work, we solve the Sasa–Satsuma equation [29,30]

$$a\psi_{xx} + b\psi\,|\psi|^2 + i(\gamma\psi(|\psi|^2)_x + \beta\psi_x\,|\psi|^2 + \alpha\psi_{xxx}) + i\psi_t = 0, \tag{1}$$

where $\psi(x,t)$ is the complex valued wave function, x, t are space and time variables, respectively, and b, γ, β, and α are real parameters. The Sasa–Satsuma equation is a higher-order nonlinear Schrödinger equation. It is significant in the field of optics as it describes the propagation of femtosecond pulses in optical fibers.

We solve the previous equation by using the $(\mathcal{H} + \frac{\mathcal{G}'}{\mathcal{G}^2})$-expansion method [31–33]. We also discuss the modulation instability and the influence of nonlinearity in modulation instability. Modulation instability refers to a phenomenon that occurs in nonlinear optical systems, particularly in optical fiber. It is a process where small perturbations in the intensity of an optical signal can grow rapidly as it propagates through the fiber [34–36]. The bifurcation and chaotic behaviors of traveling wave solutions are discussed in dynamical systems [37–41]. Atepor and Akoto [42] studied the effect of parametric force on an auto-parametric vibration absorber system. Amer *et al.* [43] investigated the vibration analysis and dynamic responses of a hybrid Rayleigh–Van der Pol–Duffing oscillator using a proportional-derivative controller. The average method was employed to obtain the approximate solution of the vibrating system.

This work is organized as follows: Sections 2 and 3 present the description and strategy of the $(\mathcal{H} + \frac{\mathcal{G}'}{\mathcal{G}^2})$-expansion method. Section 4 describes the applications of the proposed methods to find solutions to nonlinear models. Section 5 illustrates the graphical representations in 2D and 3D to show the behavior of solutions. Section 6 discusses modulation instability analysis (MIA). Section 7 exhibits bifurcation analysis. Section 8 displays the chaotic analysis. Finally, Section 9 presents the conclusion of our work.

2 Description of the method

In this section, we introduce the steps of the proposed method to show how to apply this method on Sasa–Satsuma Eq. (1). Consider the partial differential equation.

$$D = (\psi, \psi_t, \psi_x, \psi_{tt}, \psi_{xx}, \ldots), \tag{2}$$

where D represents a polynomial comprising the unknown function $\psi = \psi(x,t)$ as well as its different partial derivatives.

By using the transformation

$$\begin{aligned} \varphi(x,t) &= \zeta + t\omega + (-\kappa)x, \quad \xi = \eta(x - \nu t), \\ \psi(x,t) &= U(\xi)\exp(i\varphi(x,t)), \end{aligned} \tag{3}$$

where ω, κ, ν, ζ, η are arbitrary constants. Substitute (3) in (2), then (2) becomes ordinary differential equation as follows:

$$S = (U', U'', U''', \ldots), \tag{4}$$

where S is a polynomial in $U(\xi)$ and its derivatives.

3 Strategy of the $(\mathcal{H} + \frac{\mathcal{G}'}{\mathcal{G}^2})$-expansion approach

The essential steps of the $(\mathcal{H} + \frac{\mathcal{G}'}{\mathcal{G}^2})$-expansion technique are as follows:

Step 1: Presume the solution of (4) is given by:

$$U(\xi) = \sum_{i=-N}^{N} a_i \mathfrak{F}(\xi)^i, \tag{5}$$

where $\mathfrak{F}(\xi) = (\mathcal{H} + \frac{\mathcal{G}'(\xi)}{\mathcal{G}^2(\xi)})$, $\frac{\mathcal{G}'}{\mathcal{G}^2}$ satisfies the differential equation of second order:

$$\left(\frac{\mathcal{G}'}{\mathcal{G}^2}\right)' = A + B\left(\frac{\mathcal{G}'}{\mathcal{G}^2}\right)^2 + C\left(\frac{\mathcal{G}'}{\mathcal{G}^2}\right), \tag{6}$$

where a_i are undetermined constants, $\mathcal{A}$, B, and C are constants to be chosen later.

Step 2: Utilizing the homogeneous balance principle to determine the positive integer N.

Step 3: We procure the following classes of solutions of (6):

Class 1: When $AB > 0, C = 0$:

$$\left(\frac{\mathcal{G}'}{\mathcal{G}^2}\right) = \sqrt{\frac{A}{B}}\left(\frac{P\cos(\sqrt{AB}\,\xi) + Q\sin(\sqrt{AB}\,\xi)}{Q\cos(\sqrt{AB}\,\xi) - P\sin(\sqrt{AB}\,\xi)}\right), \tag{7}$$

where P and Q are arbitrary constants not equal to zero.

Class 2: When $AB < 0, C = 0$:

$$\left(\frac{\mathcal{G}'}{\mathcal{G}^2}\right) = -\frac{\sqrt{|AB|}}{B}\left(\frac{P\sinh(2\sqrt{|AB|}\,\xi) + P\cosh(2\sqrt{|AB|}\,\xi) + Q}{P\sinh(2\sqrt{|AB|}\,\xi) + P\cosh(2\sqrt{|AB|}\,\xi) - Q}\right). \tag{8}$$

Class 3: When $A = 0, B \neq 0, C = 0$:

$$\left(\frac{\mathcal{G}'}{\mathcal{G}^2}\right) = -\frac{P}{B(P\xi + Q)}. \tag{9}$$

Class 4: When $C^2 - 4AB \geq 0, C \neq 0$:

$$\left(\frac{\mathcal{G}'}{\mathcal{G}^2}\right) = -\frac{\sqrt{C^2 - 4AB}\left(P\cosh\left(\frac{1}{2}\xi\sqrt{C^2 - 4AB}\right) + Q\sinh\left(\frac{1}{2}\xi\sqrt{C^2 - 4AB}\right)\right)}{(2B)\left(P\sinh\left(\frac{1}{2}\xi\sqrt{C^2 - 4AB}\right) + Q\cosh\left(\frac{1}{2}\xi\sqrt{C^2 - 4AB}\right)\right)} - \frac{C}{2B}. \tag{10}$$

Class 5: When $C^2 - 4AB \le 0, C \neq 0$:

$$\left(\frac{\mathcal{G}'}{\mathcal{G}^2}\right) = -\frac{\sqrt{-C^2+4AB}\left(P\cos\left(\frac{1}{2}\xi\sqrt{-C^2+4AB}\right) - Q\sin\left(\frac{1}{2}\xi\sqrt{-C^2+4AB}\right)\right)}{(2B)\left(P\sin\left(\frac{1}{2}\xi\sqrt{-C^2+4AB}\right) + Q\cos\left(\frac{1}{2}\xi\sqrt{-C^2+4AB}\right)\right)} - \frac{C}{2B}. \tag{11}$$

Step 4: Insert (5) and (6) in (4); a system of equations is emerged as the coefficients with the same powers of $(\mathcal{H} + \frac{\mathcal{G}'}{\mathcal{G}^2})$ disappear. The Mathematica program is used to obtain the solution of this system.

4 Applications of methods

By inserting (3) into (1) and equating the real and imaginary parts to zero, we obtain

$$\begin{aligned}&\eta(\eta((3a\kappa + a)U''(\xi) + ia\eta U^{(3)}(\xi))\\ &\quad - iU'(\xi)(3a\kappa^2 + 2a\kappa + v)) - U(\xi)(\kappa^2(a\kappa + a) + \omega)\\ &\quad + U(\xi)^3(\beta\kappa + b) + i\eta(\beta + 2\gamma)U(\xi)^2U'(\xi) = 0.\end{aligned} \tag{12}$$

A real part is obtained as

$$\begin{aligned}&\eta^2(3a\kappa + a)U''(\xi) - U(\xi)(a\kappa^3 + a\kappa^2 + \omega)\\ &\quad + U(\xi)^3(\beta\kappa + b) = 0,\end{aligned} \tag{13}$$

and imaginary part is given by

$$\begin{aligned}&-U(\xi)(3a\kappa^2 + 2a\kappa + v) + a\eta^2U''(\xi) + \frac{1}{3}(\beta + 2\gamma)U(\xi)^3\\ &\quad = 0.\end{aligned} \tag{14}$$

Equating the coefficients of $U(\xi)$, $U(\xi)^3$, and $U''(\xi)$ in Eqs (13) and (14), respectively, we obtain the following:

$$\begin{aligned}\omega &= \frac{v(3a\kappa + a) + 2\kappa(2a\kappa + a)^2}{a},\\ b &= \frac{a(\beta + 2\gamma)}{3a} + 2\gamma\kappa.\end{aligned} \tag{15}$$

We balance $U(\xi)^3$, and $U''(\xi)$ in Eq. (13), then, we obtain $N = 1$.

4.1 Solution of $(\mathcal{H} + \frac{\mathcal{G}'}{\mathcal{G}^2})$-expansion approach

Substitute (5) and (6) in (13) with $N = 1$, then collect all terms that have the same power of $(\mathcal{H} + \frac{\mathcal{G}'}{\mathcal{G}^2})$ and equate them to zero, we obtain the following system:

$$\begin{aligned}&-\frac{2a^2a_0\kappa}{a} + \frac{aa_0^3\beta}{3a} + \frac{2aa_{-1}a_0a_1\beta}{a} + \frac{2aa_0^3\gamma}{3a} + \frac{4aa_{-1}a_0a_1\gamma}{a}\\ &\quad - 9aa_0\kappa^3 - \frac{aa_0\nu}{a} - 6aa_1AB\eta^2\kappa\mathcal{H} - 2aa_1AB\eta^2\mathcal{H}\\ &\quad + 3aa_1AC\eta^2\kappa + aa_1AC\eta^2 + a_0^3\beta\kappa + 6a_{-1}a_0a_1\beta\kappa\\ &\quad - 6aa_1B^2\eta^2\kappa\mathcal{H}^3 - 2aa_1B^2\eta^2\mathcal{H}^3 - 6aa_{-1}B^2\eta^2\kappa\mathcal{H}\\ &\quad - 2aa_{-1}B^2\eta^2\mathcal{H} + 3aa_{-1}BC\eta^2\kappa + aa_{-1}BC\eta^2\\ &\quad + 9aa_1BC\eta^2\kappa\mathcal{H}^2 + 3aa_1BC\eta^2\mathcal{H}^2 + 2a_0^3\gamma\kappa + 12a_{-1}a_0a_1\gamma\kappa\\ &\quad - 3aa_1C^2\eta^2\kappa\mathcal{H} - aa_1C^2\eta^2\mathcal{H} - 9aa_0\kappa^2 - 3a_0\kappa\nu = 0,\end{aligned}$$

$$\begin{aligned}&\frac{aa_{-1}^3\beta}{3a} + \frac{2aa_{-1}^3\gamma}{3a} + 6aa_{-1}A^2\eta^2\kappa\\ &\quad + 2aa_{-1}A^2\eta^2 + 12aa_{-1}AB\eta^2\kappa\mathcal{H}^2 + 4aa_{-1}AB\eta^2\mathcal{H}^2\\ &\quad - 12aa_{-1}AC\eta^2\kappa\mathcal{H} - 4aa_{-1}AC\eta^2\mathcal{H} + a_{-1}^3\beta\kappa\\ &\quad + 6aa_{-1}B^2\eta^2\kappa\mathcal{H}^4 + 2aa_{-1}B^2\eta^2\mathcal{H}^4 - 12aa_{-1}BC\eta^2\kappa\mathcal{H}^3\\ &\quad - 4aa_{-1}BC\eta^2\mathcal{H}^3 + 2a_{-1}^3\gamma\kappa + 6aa_{-1}C^2\eta^2\kappa\mathcal{H}^2\\ &\quad + 2aa_{-1}C^2\eta^2\mathcal{H}^2 = 0,\end{aligned}$$

$$\begin{aligned}&\frac{aa_{-1}^2a_0\beta}{a} + \frac{2aa_{-1}^2a_0\gamma}{a} - 18aa_{-1}AB\eta^2\kappa\mathcal{H}\\ &\quad - 6aa_{-1}AB\eta^2\mathcal{H} + 9aa_{-1}AC\eta^2\kappa\\ &\quad + 3aa_{-1}AC\eta^2 + 3a_{-1}^2a_0\beta\kappa - 18aa_{-1}B^2\eta^2\kappa\mathcal{H}^3\\ &\quad - 6aa_{-1}B^2\eta^2\mathcal{H}^3 + 27aa_{-1}BC\eta^2\kappa\mathcal{H}^2 + 9aa_{-1}BC\eta^2\mathcal{H}^2\\ &\quad + 6a_{-1}^2a_0\gamma\kappa - 9aa_{-1}C^2\eta^2\kappa\mathcal{H} - 3aa_{-1}C^2\eta^2\mathcal{H} = =0,\end{aligned}$$

$$\begin{aligned}&-\frac{2a^2a_{-1}\kappa}{a} + \frac{aa_{-1}a_0^2\beta}{a} + \frac{aa_{-1}^2a_1\beta}{a}\\ &\quad + \frac{2aa_{-1}a_0^2\gamma}{a} + \frac{2aa_{-1}^2a_1\gamma}{a} - 9aa_{-1}\kappa^3\\ &\quad - \frac{aa_{-1}\nu}{a} + 6aa_{-1}AB\eta^2\kappa + 2aa_{-1}AB\eta^2 + 3a_{-1}a_0^2\beta\kappa\\ &\quad + 3a_{-1}^2a_1\beta\kappa + 18aa_{-1}B^2\eta^2\kappa\mathcal{H}^2 + 6aa_{-1}B^2\eta^2\mathcal{H}^2\\ &\quad - 18aa_{-1}BC\eta^2\kappa\mathcal{H} - 6aa_{-1}BC\eta^2\mathcal{H} + 6a_{-1}a_0^2\gamma\kappa\\ &\quad + 6a_{-1}^2a_1\gamma\kappa + 3aa_{-1}C^2\eta^2\kappa + aa_{-1}C^2\eta^2 - 9aa_{-1}\kappa^2 - 3a_{-1}\kappa\nu\\ &\quad = 0,\end{aligned}$$

$$
\begin{aligned}
&-\frac{2a^2a_1\kappa}{\alpha}+\frac{aa_{-1}a_1^2\beta}{\alpha}+\frac{aa_0^2a_1\beta}{\alpha}+\frac{2aa_{-1}a_1^2\gamma}{\alpha}\\
&+\frac{2aa_0^2a_1\gamma}{\alpha}-9aa_1\kappa^3-\frac{aa_1\nu}{\alpha}+6aa_1AB\eta^2\kappa\\
&+2aa_1AB\eta^2+3a_{-1}a_1^2\beta\kappa+3a_0^2a_1\beta\kappa+18aa_1B^2\eta^2\kappa\mathcal{H}^2\\
&+6aa_1B^2\eta^2\mathcal{H}^2-18aa_1BC\eta^2\kappa\mathcal{H}-6aa_1BC\eta^2\mathcal{H}\\
&+6a_{-1}a_1^2\gamma\kappa+6a_0^2a_1\gamma\kappa+3aa_1C^2\eta^2\kappa\\
&+aa_1C^2\eta^2-9aa_1\kappa^2-3a_1\kappa\nu=0,
\end{aligned}
$$

$$
\begin{aligned}
&\frac{aa_0a_1^2\beta}{\alpha}+\frac{2aa_0a_1^2\gamma}{\alpha}+3a_0a_1^2\beta\kappa-18aa_1B^2\eta^2\kappa\mathcal{H}\\
&-6aa_1B^2\eta^2\mathcal{H}+9aa_1BC\eta^2\kappa+3aa_1BC\eta^2+6a_0a_1^2\gamma\kappa=0,
\end{aligned}
$$

$$
\begin{aligned}
&\frac{aa_1^3\beta}{3\alpha}+\frac{2aa_1^3\gamma}{3\alpha}+a_1^3\beta\kappa+6aa_1B^2\eta^2\kappa\\
&+2aa_1B^2\eta^2+2a_1^3\gamma\kappa=0.
\end{aligned}
$$

Solving the above system of equations, we obtain the following sets of solutions: **set 1**.

$$
\begin{aligned}
a_0&=\frac{a_1C-2a_1B\mathcal{H}}{2B},\quad a_{-1}=0,\\
\beta&=-\frac{2(a_1^2\gamma+3aB^2\eta^2)}{a_1^2},\\
a&=\frac{-6a\kappa^2+4aAB\eta^2+a(-C^2)\eta^2-2\nu}{4\kappa}.
\end{aligned}
\tag{16}
$$

set 2.

$$
\begin{aligned}
a_1&=0,\quad a_{-1}=-\frac{2a_0(-A-B\mathcal{H}^2+C\mathcal{H})}{C-2B\mathcal{H}},\\
a&=\frac{-6a\kappa^2+4aAB\eta^2+a(-C^2)\eta^2-2\nu}{4\kappa},\\
\beta&=\frac{-4a_0^2\gamma-12aB^2\eta^2\mathcal{H}^2+12aBC\eta^2\mathcal{H}-3aC^2\eta^2}{2a_0^2}.
\end{aligned}
\tag{17}
$$

By substituting the values from Eqs (16) and (17) in Eq. (5) and utilizing Eqs (7)–(11), we can determine $U(\xi)$. Subsequently, by substituting $U(\xi)$ in Eq. (3), we can obtain the solutions of Eq. (1) as follows:

Class 1: When $AB>0, C=0$:

$$
\begin{aligned}
\psi(x,t)=&\left[a_0+a_1\left(\mathcal{H}+\sqrt{\frac{A}{B}}\left(\frac{P\cos(\sqrt{AB}\,\xi)+Q\sin(\sqrt{AB}\,\xi)}{Q\cos(\sqrt{AB}\,\xi)-P\sin(\sqrt{AB}\,\xi)}\right)\right)\right.\\
&\left.+a_{-1}\left(\mathcal{H}+\sqrt{\frac{A}{B}}\left(\frac{P\cos(\sqrt{AB}\,\xi)+Q\sin(\sqrt{AB}\,\xi)}{Q\cos(\sqrt{AB}\,\xi)-P\sin(\sqrt{AB}\,\xi)}\right)\right)^{-1}\right]\exp(i(\zeta+t\omega+(-\kappa)x)).
\end{aligned}
\tag{18}
$$

Class 2: When $AB<0, C=0$:

$$
\begin{aligned}
\psi(x,t)=&\left[a_0+a_1\left(\mathcal{H}-\frac{\sqrt{|AB|}}{B}\left(\frac{P\sinh(2\sqrt{|AB|}\,\xi)+P\cosh(2\sqrt{|AB|}\,\xi)+Q}{P\sinh(2\sqrt{|AB|}\,\xi)+P\cosh(2\sqrt{|AB|}\,\xi)-Q}\right)\right)\right.\\
&\left.+a_{-1}\left(\mathcal{H}-\frac{\sqrt{|AB|}}{B}\left(\frac{P\sinh(2\sqrt{|AB|}\,\xi)+P\cosh(2\sqrt{|AB|}\,\xi)+Q}{P\sinh(2\sqrt{|AB|}\,\xi)+P\cosh(2\sqrt{|AB|}\,\xi)-Q}\right)\right)^{-1}\right]\exp(i(\zeta+t\omega+(-\kappa)x)).
\end{aligned}
\tag{19}
$$

Class 3: When $A=0, B\neq 0, C=0$:

$$
\psi(x,t)=\left[a_0+a_1\left(\mathcal{H}-\frac{P}{B(P\xi+Q)}\right)+a_{-1}\left(\mathcal{H}-\frac{P}{B(P\xi+Q)}\right)^{-1}\right]\exp(i(\zeta+t\omega+(-\kappa)x)).
\tag{20}
$$

Class 4: When $C^2-4AB\geq 0, C\neq 0$:

$$
\begin{aligned}
\psi(x,t)=&\left[a_0+a_1\left(\mathcal{H}-\frac{\sqrt{C^2-4AB}\left(P\cosh\left(\frac{1}{2}\xi\sqrt{C^2-4AB}\right)+Q\sinh\left(\frac{1}{2}\xi\sqrt{C^2-4AB}\right)\right)}{(2B)\left(P\sinh\left(\frac{1}{2}\xi\sqrt{C^2-4AB}\right)+Q\cosh\left(\frac{1}{2}\xi\sqrt{C^2-4AB}\right)\right)}-\frac{C}{2B}\right)\right.\\
&\left.+a_{-1}\left(\mathcal{H}-\frac{\sqrt{C^2-4AB}\left(P\cosh\left(\frac{1}{2}\xi\sqrt{C^2-4AB}\right)+Q\sinh\left(\frac{1}{2}\xi\sqrt{C^2-4AB}\right)\right)}{(2B)\left(P\sinh\left(\frac{1}{2}\xi\sqrt{C^2-4AB}\right)+Q\cosh\left(\frac{1}{2}\xi\sqrt{C^2-4AB}\right)\right)}-\frac{C}{2B}\right)^{-1}\right]\exp(i(\zeta+t\omega+(-\kappa)x)).
\end{aligned}
\tag{21}
$$

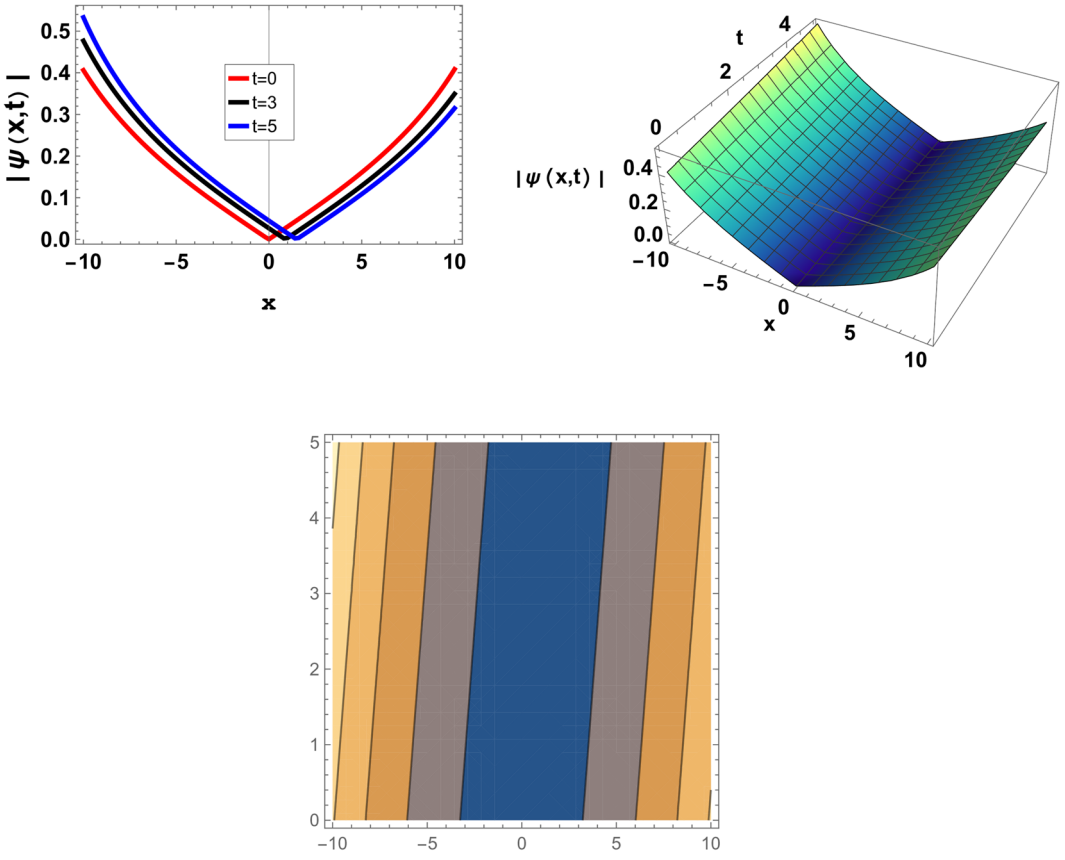

Figure 1: The graph of (18) with (16) at $\alpha = 0.4$, $a_1 = 0.2$, $A = 1.5$, $B = 0.5$, $\gamma = 0.1$, $C = 0$, $\zeta = 0$, $\eta = 0.1$, $\kappa = 0.3$, $\nu = 0.3$, $P = 0.01$, $Q = 7$, and $\mathcal{H} = 0.5$.

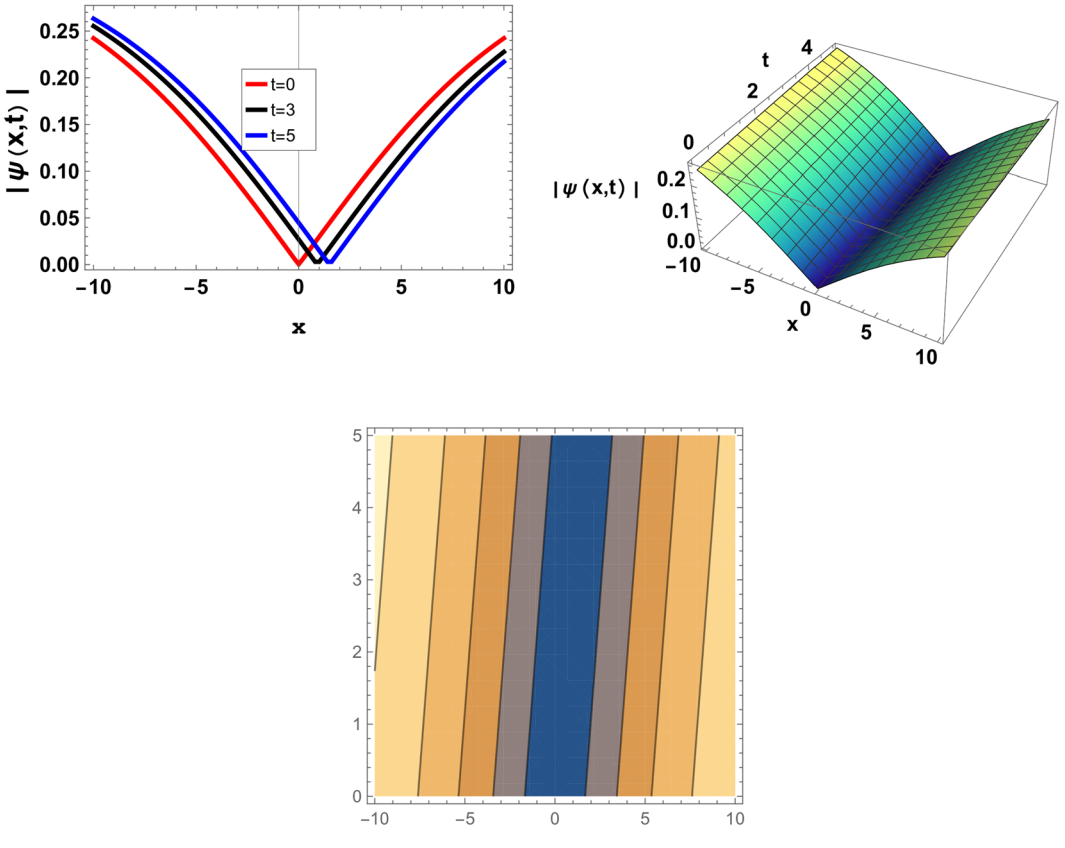

Figure 2: The graph of (19) with (16) at $\alpha = 0.4$, $a_1 = 0.2$, $A = -1.5$, $B = 0.5$, $\gamma = 0.1$, $C = 0$, $\zeta = 0$, $\eta = 0.1$, $\kappa = 0.3$, $\nu = 0.3$, $P = 0.01$, $Q = 7$, and $\mathcal{H} = 0.5$.

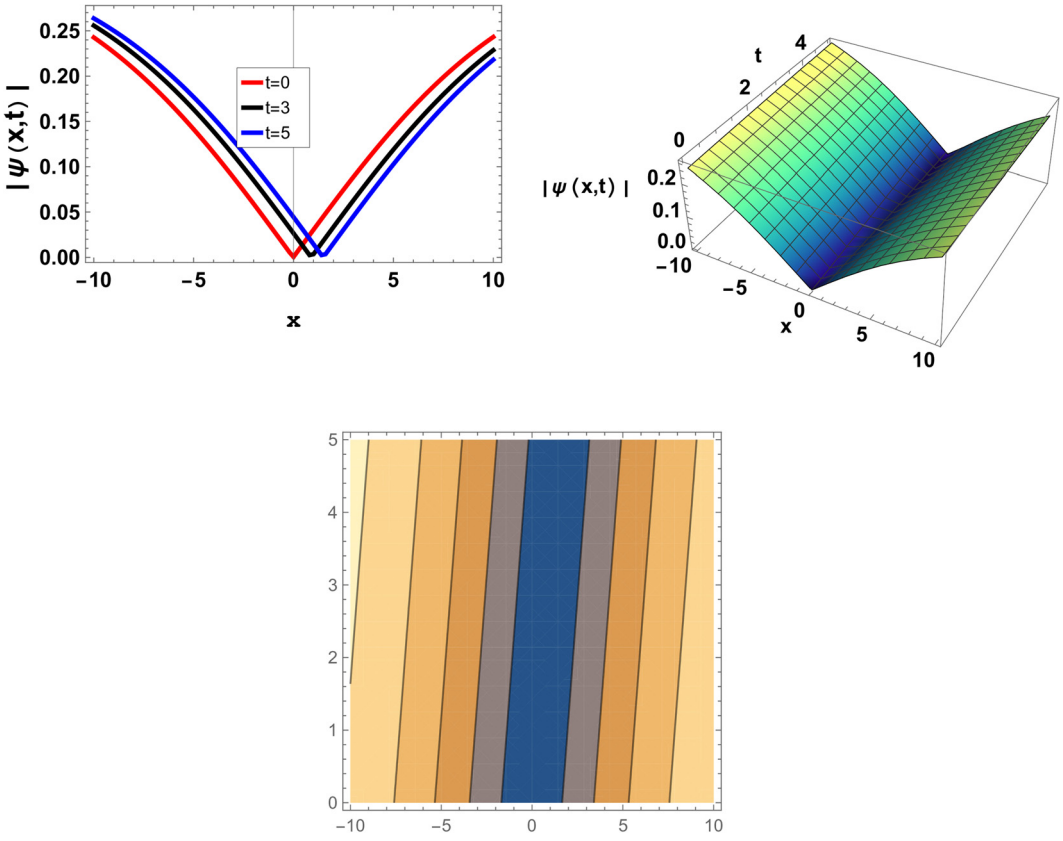

Figure 3: The graph of (21) with (16) at $\alpha = 0.4$, $a_1 = 0.2$, $A = -1.5$, $B = 0.5$, $\gamma = 0.1$, $C = 0.1$, $\zeta = 0$, $\eta = 0.1$, $\kappa = 0.3$, $\nu = 0.3$, $P = 0.01$, $Q = 7$, and $\mathcal{H} = 0.5$.

Class 5: When $C^2 - 4AB \le 0$, $C \neq 0$:

$$\psi(x,t) = \left[a_0 + a_1 \left(\mathcal{H} - \frac{\sqrt{-C^2+4AB}\left(P\cos\left(\frac{1}{2}\xi\sqrt{-C^2+4AB}\right) - Q\sin\left(\frac{1}{2}\xi\sqrt{-C^2+4AB}\right)\right)}{(2B)\left(P\sin\left(\frac{1}{2}\xi\sqrt{-C^2+4AB}\right) + Q\cos\left(\frac{1}{2}\xi\sqrt{-C^2+4AB}\right)\right)} - \frac{C}{2B} \right) \right.$$
$$\left. + a_{-1}\left(\mathcal{H} - \frac{\sqrt{-C^2+4AB}\left(P\cos\left(\frac{1}{2}\xi\sqrt{-C^2+4AB}\right) - Q\sin\left(\frac{1}{2}\xi\sqrt{-C^2+4AB}\right)\right)}{(2B)\left(P\sin\left(\frac{1}{2}\xi\sqrt{-C^2+4AB}\right) + Q\cos\left(\frac{1}{2}\xi\sqrt{-C^2+4AB}\right)\right)} - \frac{C}{2B} \right)^{-1} \right] \exp(i(\zeta + t\omega + (-\kappa)x)). \tag{22}$$

5 Graphical illustrations

In this section, we introduce some figures in the two-dimension (2D) and three-dimension (3D) about some solutions of NPDE by the $(\mathcal{H} + \frac{\mathcal{G}'}{\mathcal{G}^2})$- expansion method. In Figure 1, we introduce the graph of (18) with (16) at $\alpha = 0.4$, $a_1 = 0.2$, $A = 1.5$, $B = 0.5$, $\gamma = 0.1$, $C = 0$, $\zeta = 0$, $\eta = 0.1$, $\kappa = 0.3$, $\nu = 0.3$, $P = 0.01$, $Q = 7$, and $\mathcal{H} = 0.5$. The graph of (19) with (16) at $\alpha = 0.4$, $a_1 = 0.2$, $A = -1.5$, $B = 0.5$, $\gamma = 0.1$, $C = 0$, $\zeta = 0$, $\eta = 0.1$, $\kappa = 0.3$, $\nu = 0.3$, $P = 0.01$, $Q = 7$, and $\mathcal{H} = 0.5$ is presented in Figure 2. In Figure 3, we introduce the graph of (21) with (16) at $\alpha = 0.4$, $a_1 = 0.2$, $A = -1.5$, $B = 0.5$, $\gamma = 0.1$, $C = 0.1$, $\zeta = 0$, $\eta = 0.1$, $\kappa = 0.3$, $\nu = 0.3$, $P = 0.01$, $Q = 7$, and $\mathcal{H} = 0.5$. The graph of (21) with (16) at $a_1 = 0.001$, $\alpha = 0.4$, $A = 0.5$, $B = 0.8$, $\gamma = 0.6$, $C = 0.6$, $\zeta = 0$, $\eta = 0.001$, $\kappa = 0.1$, $\nu = 0.3$, $P = 0.001$, $Q = 7$, and $\mathcal{H} = 0.01$ is presented in Figure 4. In Figure 5, we introduce the graph of (18) with (17) at $\alpha = 0.01$, $a_0 = 0.0001$, $A = 1.4$, $B = 0.5$, $\gamma = 0.1$, $C = 0$, $\zeta = 0$, $\eta = 0.1$, $\kappa = 4$, $\nu = 0.8$, $P = 4$, $Q = 11$, and $\mathcal{H} = 0.1$. The graph of (19) with (17) at $\alpha = 0.01$, $a_0 = 0.01$, $A = 1.1$, $B = -0.5$, $\gamma = 0.1$, $C = 0$, $\zeta = 0$, $\eta = 0.1$, $\kappa = 4$, $\nu = 0.5$, $P = 4$, $Q = 7$, $\mathcal{H} = 0.1$ is presented in Figure 6. In Figure 7, we introduce the graph of (21) with (17) at $\alpha = 0.4$, $a_0 = 0.001$, $A = -0.5$, $B = 0.7$, $\gamma = 0.1$, $C = 0.1$, $\zeta = 0$, $\eta = 0.1$, $\kappa = 0.3$, $\nu = 0.3$, $P = 4$, $Q = 2.5$, and $\mathcal{H} = 0.5$.

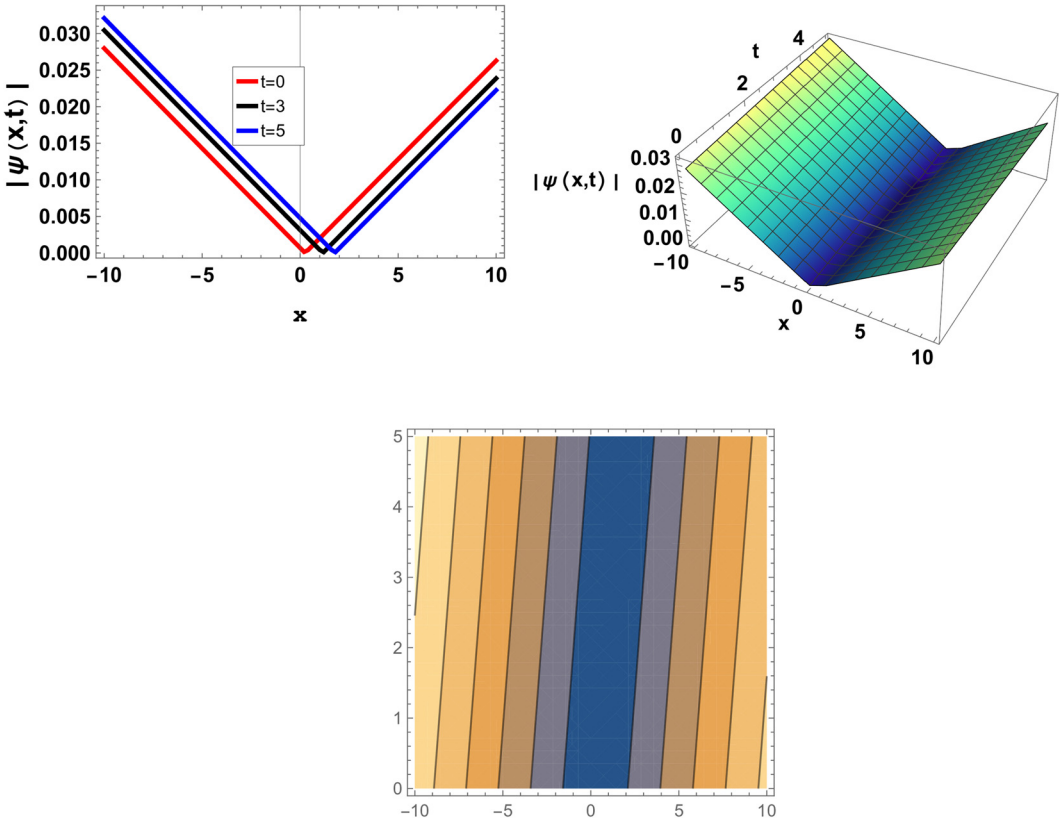

Figure 4: The graph of (21) with (16) at $a_1 = 0.001$, $\alpha = 0.4$, $A = 0.5$, $B = 0.8$, $\gamma = 0.6$, $C = 0.6$, $\zeta = 0$, $\eta = 0.001$, $\kappa = 0.1$, $\nu = 0.3$, $P = 0.001$, $Q = 7$, and $\mathcal{H} = 0.01$.

The graph of (21) with (17) at $\alpha = 0.4$, $a_0 = 0.001$, $A = 0.3$, $B = 0.4$, $\gamma = 0.1$, $C = 0.5$, $\zeta = 0$, $\eta = 0.3$, $\kappa = 0.4$, $\nu = 0.3$, $P = 9$, $Q = 8$, and $\mathcal{H} = 0.1$ is presented in Figure 8. We give 2D, 3D, and contour plots of the derived solutions that illustrate several soliton types, including dark, bright, and singular traveling wave solutions in optical fibers.

6 MIA

Modulation instability (MI) refers to a phenomenon that occurs in nonlinear optical systems, particularly in optical fibers. It is a process where small perturbations or fluctuations in an optical signal can grow rapidly, leading to the formation of multiple distinct pulses within the signal. This instability arises due to the interplay between the nonlinear effects in the medium and the dispersion of the signal. MI is used to display the behavior of the continuous waves over a long time of evolution.

We suppose the following plane-wave as solution of (1):

$$\psi(x,t) = p_0 \exp(i(\delta x - t\omega)), \tag{23}$$

where p_0 is the input signal, δ is the wave vector, and ω is the angular frequency. Substituting (23) in (1), we obtain the linear dispersion as follows:

$$\omega = \delta^2(a - a\delta) + p_0^2(\beta\delta - b). \tag{24}$$

To obtain the linearized expression, one introduces the tiny perturbations in the plane-wave

$$\psi(x,t) = (\mu(x,t) + p_0)\exp(i(\delta x - t\omega)), \tag{25}$$

where $\mu(x,t)$ is the perturbed amplitude. Substituting (24) and (25) in (1), we obtain the following equation:

$$\begin{aligned} &2a\delta\mu_x(x,t) - ia\mu_{xx}(x,t) + p_0^2(-i(b-\beta\delta)\mu(x,t) \\ &\quad - i(b-\beta\delta)\mu^*(x,t) + (\beta+\gamma)\mu_x(x,t) + \gamma\mu_x^*(x,t)) \\ &\quad - 3a\delta^2\mu_x(x,t) + 3ia\delta\mu_{xx}(x,t) + a\mu_{xxx}(x,t) \\ &\quad + \mu_t(x,t) = 0, \end{aligned} \tag{26}$$

where μ^* is the complex conjugate of $\mu(x,t)$. While $\mu(x,t)$ is the small perturbation and expressed as follows:

$$\mu(x,t) = f_1 \exp(i(Kx - \Omega t)) + f_2 \exp(-i(Kx - \Omega t)), \tag{27}$$

where K is the real disturbance wave-number, Ω is the complex frequency, and f_1, f_2 are the coefficients of linear combination. Substituting (27) in (26), we may have the following homogeneous equations:

$$\begin{aligned} &f_1(-aK(2\delta + K) + aK^3 + 3a\delta K^2 + 3a\delta^2 K + \Omega) \\ &\quad + p_0^2(b(f_1 + f_2) - f_1(\beta\delta + K(\beta + \gamma)) - f_2(\beta\delta + \gamma K)) = 0, \\ &f_2(aK(K - 2\delta) + aK^3 - 3a\delta K^2 + 3a\delta^2 K + \Omega) \\ &\quad - p_0^2(b(f_1 + f_2) - \beta\delta f_1 + \gamma f_1 K - \beta\delta f_2 + \beta f_2 K + \gamma f_2 K) = 0. \end{aligned} \tag{28}$$

We evaluate the determinate of the above system and setting to zero, we obtain two-order polynomial equation

$$\Omega^2 + \Lambda_1\Omega + \Lambda_0 = 0, \tag{29}$$

where

$$\begin{aligned} \Lambda_0 = &-a^2K^4 + 4a^2\delta^2K^2 + 2abK^2p_0^2 \\ &+ 2aa\delta K^4 - 12aa\delta^3K^2 + 2a\beta\delta K^2p_0^2 \\ &+ 4a\gamma\delta K^2p_0^2 - 6ab\delta K^2p_0^2 + a^2K^6 \\ &- 3a^2\delta^2K^4 - 2a\beta K^4p_0^2 - 2a\gamma K^4p_0^2 \\ &+ 9a^2\delta^4K^2 - 6a\gamma\delta^2K^2p_0^2 + \beta^2K^2p_0^4 + 2\beta\gamma K^2p_0^4, \\ \Lambda_1 = &-4a\delta K + 2aK^3 + 6a\delta^2K - 2\beta Kp_0^2 - 2\gamma Kp_0^2, \end{aligned} \tag{30}$$

and the MI growth rate is as follows:

$$\sigma = |\mathrm{Im}[\Omega_{\max}]|. \tag{31}$$

Considering (29), the following cases of the modulation instability of (1) can be discussed as follows:

$$\begin{aligned} \Omega = \mp &\sqrt{a^2K^4 - 2abK^2p_0^2 - 6aa\delta K^4 + 2a\beta\delta K^2p_0^2} \\ &\sqrt{+ 6ab\delta K^2p_0^2 + 9a^2\delta^2K^4 - 6a\beta\delta^2K^2p_0^2 + \gamma^2K^2p_0^4} \\ &+ 2a\delta K - aK^3 - 3a\delta^2K + \beta Kp_0^2 + \gamma Kp_0^2. \end{aligned} \tag{32}$$

The stability of the steady state is determined by (32). When Ω has an imaginary part, then steady-state solution is unstable because the perturbation rises exponentially. But if the wave number Ω is real, the steady state is stable against small perturbations. Thus, the modulation instability of (32) takes place when

$$\begin{aligned} &a^2K^4 - 2abK^2p_0^2 - 6aa\delta K^4 + 2a\beta\delta K^2p_0^2 \\ &\quad + 6ab\delta K^2p_0^2 + 9a^2\delta^2K^4 - 6a\beta\delta^2K^2p_0^2 \\ &\quad + \gamma^2K^2p_0^4 < 0. \end{aligned} \tag{33}$$

Eventually, we attain the MI gain spectrum as

$$\begin{aligned} G(K) &= 2Im(\Omega) \\ &= 2\mathrm{Im}\sqrt{a^2K^4 - 2abK^2p_0^2 - 6aa\delta K^4 + 2a\beta\delta K^2p_0^2} \\ &\quad \sqrt{+ 6ab\delta K^2p_0^2 + 9a^2\delta^2K^4 - 6a\beta\delta^2K^2p_0^2 + \gamma^2K^2p_0^4}. \end{aligned} \tag{34}$$

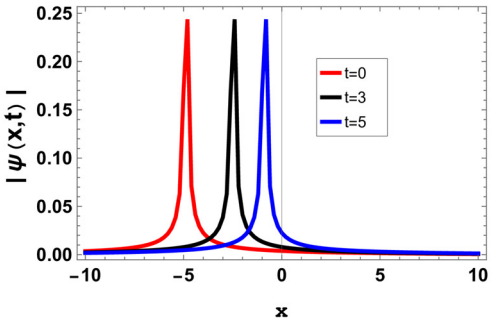

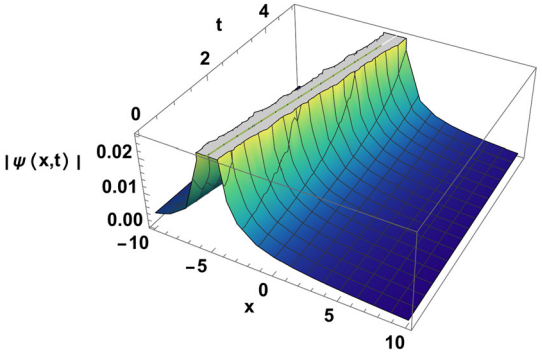

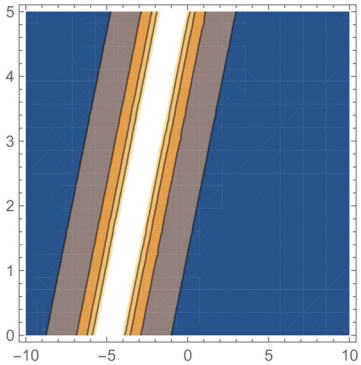

Figure 5: The graph of (18) with (17) at $\alpha = 0.01, a_0 = 0.0001, A = 1.4, B = 0.5, \gamma = 0.1, C = 0, \zeta = 0, \eta = 0.1, \kappa = 4, \nu = 0.8, P = 4, Q = 11$, and $\mathcal{H} = 0.1$.

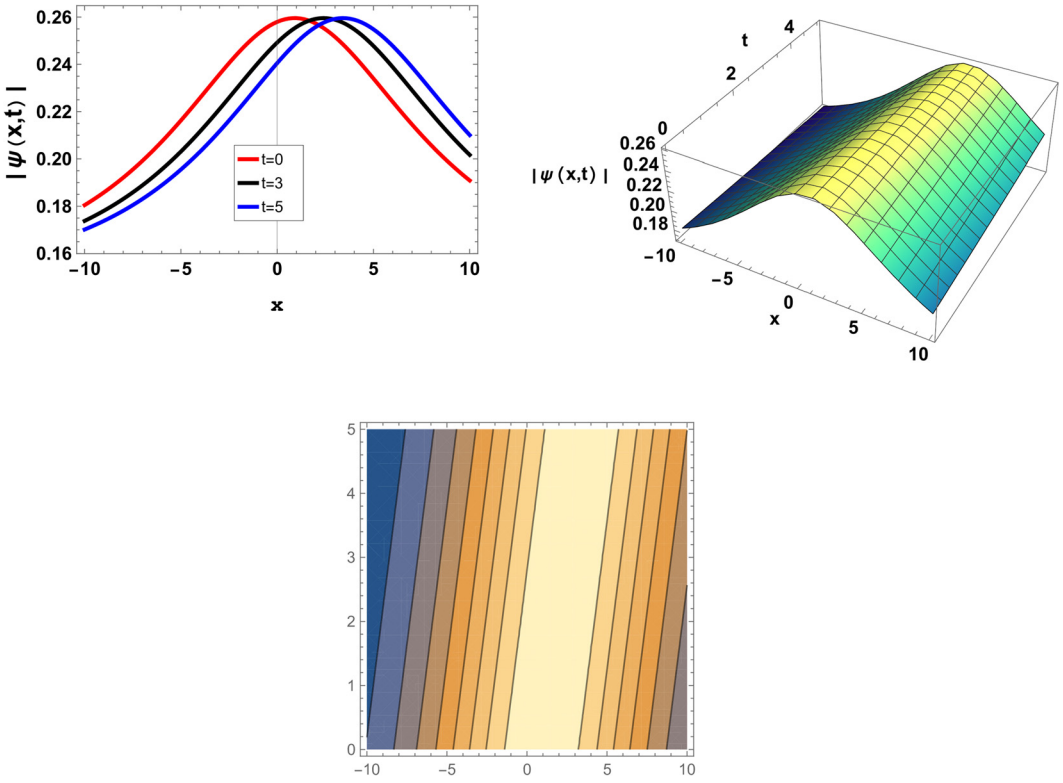

Figure 6: The graph of (19) with (17) at $\alpha = 0.01$, $a_0 = 0.01$, $A = 1.1$, $B = -0.5$, $\gamma = 0.1$, $C = 0$, $\zeta = 0$, $\eta = 0.1$, $\kappa = 4$, $\nu = 0.5$, $P = 4$, $Q = 7$, and $\mathcal{H} = 0.1$.

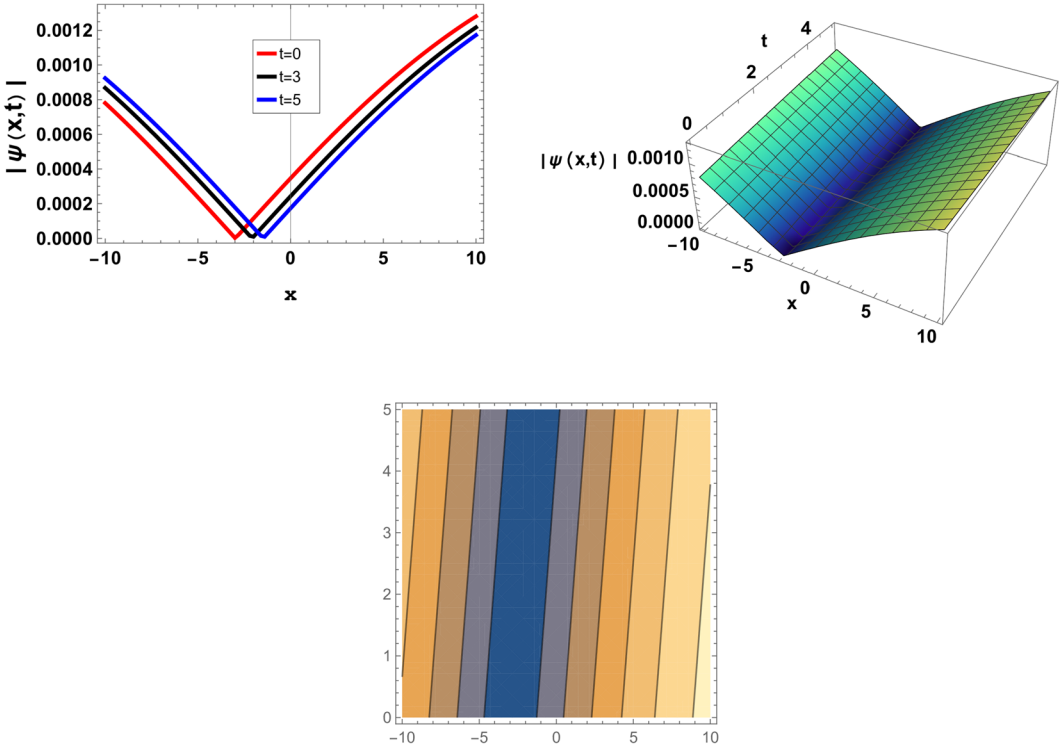

Figure 7: The graph of (21) with (17) at $\alpha = 0.4$, $a_0 = 0.001$, $A = -0.5$, $B = 0.7$, $\gamma = 0.1$, $C = 0.1$, $\zeta = 0$, $\eta = 0.1$, $\kappa = 0.3$, $\nu = 0.3$, $P = 4$, $Q = 2.5$, and $\mathcal{H} = 0.5$.

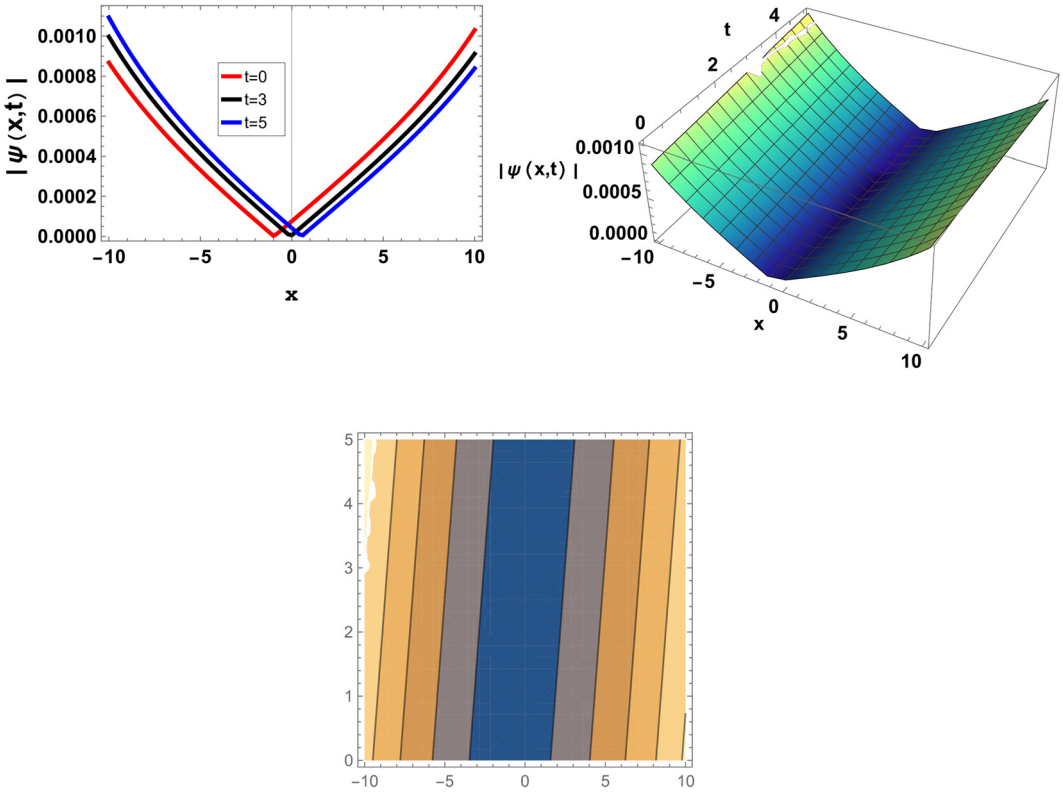

Figure 8: The graph of (21) with (17) at $\alpha = 0.4, a_0 = 0.001, A = 0.3, B = 0.4, \gamma = 0.1, C = 0.5, \zeta = 0, \eta = 0.3, \kappa = 0.4, \nu = 0.3, P = 9, Q = 8$, and $\mathcal{H} = 0.1$.

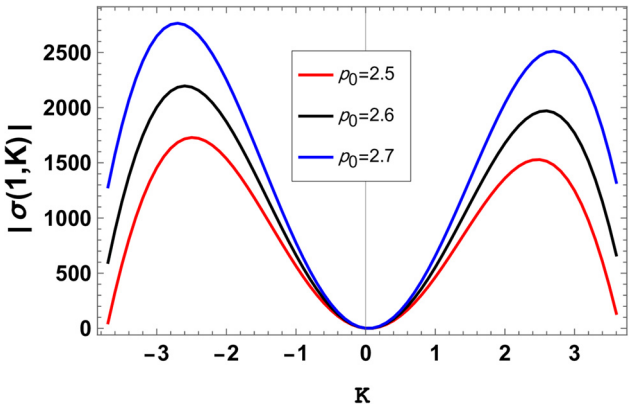

Figure 9: The 2D graph of (29) for the values of $\alpha = 1, a = 1, b = 2, \beta = 2.5, \delta = 0.9$, and $\gamma = 1.8$.

In the following figures, we show that modulation instability is significantly affected by changing the parameters.

Modulation instability refers to the phenomenon where small perturbations in an optical signal can grow exponentially, leading to the formation of multiple distinct pulses. This is particularly significant in optical fibers, where nonlinear effects interact with dispersion. Figures 9–13 collectively illustrate how modulation instability manifests in optical systems. Varying parameters like nonlinearity and dispersion can create different growth patterns, reinforcing the importance of understanding these interactions for applications in nonlinear optics and fiber communications.

7 Bifurcation analysis

In this section, we transform Eq. (13) into a planar dynamical system using bifurcation theory [37], to obtain the following system:

$$\begin{aligned} U'(\xi) &= W(\xi), \\ W'(\xi) &= \frac{1}{\mathcal{A}_1}(\mathcal{A}_2 U(\xi) - \mathcal{A}_3 (U(\xi))^3), \end{aligned} \tag{35}$$

where $\mathcal{A}_1 = \eta^2(3a\kappa + a)$, $\mathcal{A}_2 = a\kappa^3 + a\kappa^2 + \omega$, and $\mathcal{A}_3 = \beta\kappa + b$.

It is important to show that the set of differential Eq. (35) is a conservative system if $\vec{\nabla}.\vec{\mathcal{F}} = 0$, such that $\vec{\mathcal{F}} = W\vec{i} + \frac{1}{\mathcal{A}_1}(\mathcal{A}_2 U - \mathcal{A}_3 U^3)\vec{j}$ is a vector field and constitutes the Hamiltonian function. The Hamiltonian function represents the total energy of system (35) (kinetic energy and potential energy), can be defined as follows:

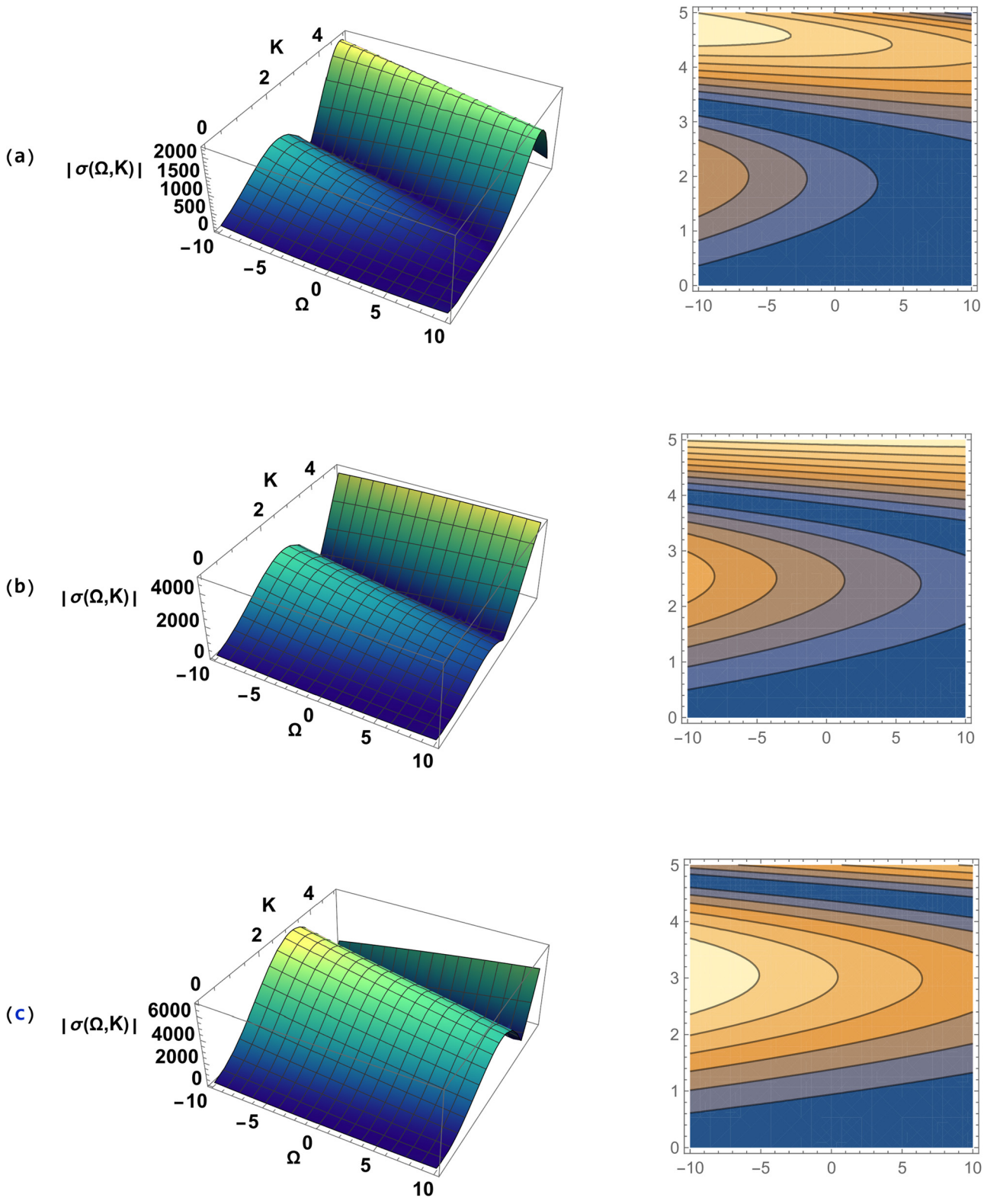

Figure 10: The 3D graph of (29) for the values of $\alpha = 1$, $a = 1$, $b = 2$, $\beta = 2.5$, $\delta = 0.9$, $\gamma = 1.8$ with (a) $p_0 = 2$, (b) $p_0 = 2.5$, and (c) $p_0 = 3$..

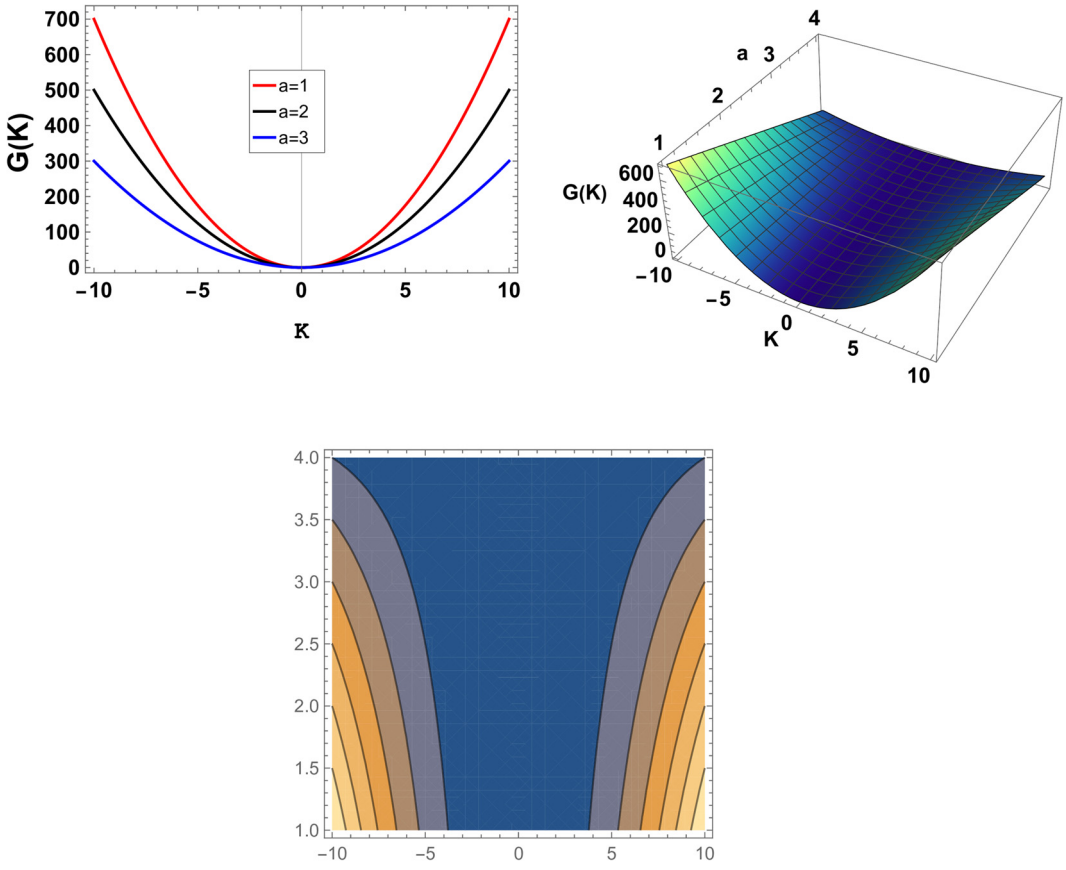

Figure 11: The graph of (34) for the values of $\alpha = 0.3$, $\beta = 0.5$, $b = 3$, $\gamma = 5$, $\delta = 5$, and $p_0 = 0.1$.

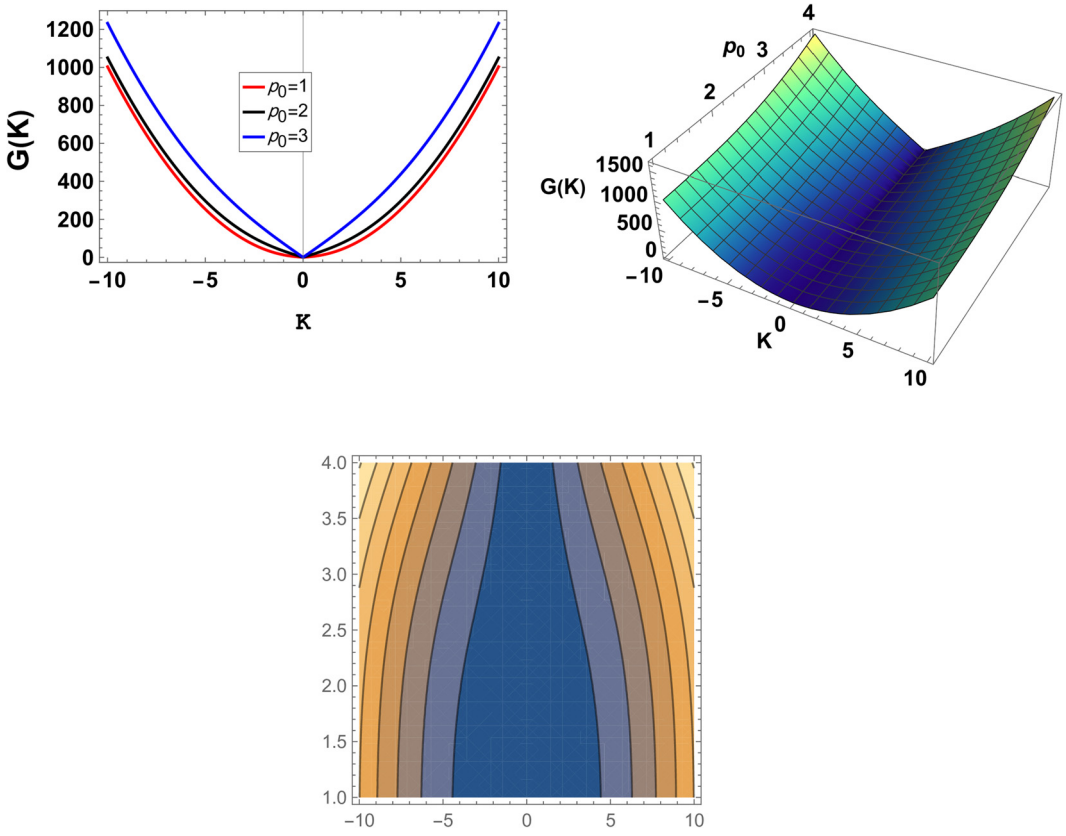

Figure 12: The graph of (34) for the values of $\alpha = 2$, $a = 1$, $\beta = 2$, $b = 2$, $\gamma = 4$, and $\delta = 1$.

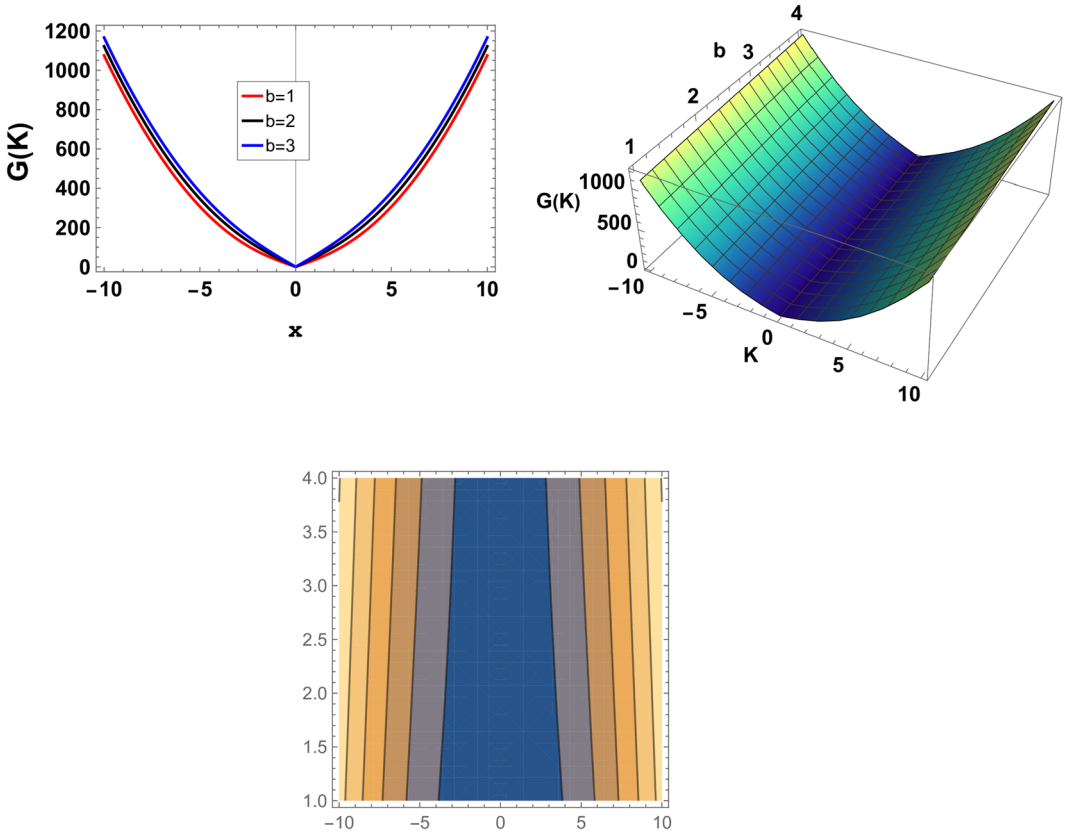

Figure 13: The graph of (34) for the values of $\alpha = 2$, $a = 1.5$, $\beta = 1.3$, $\gamma = 0.8$, $\delta = 1.1$, and $p_0 = 5$.

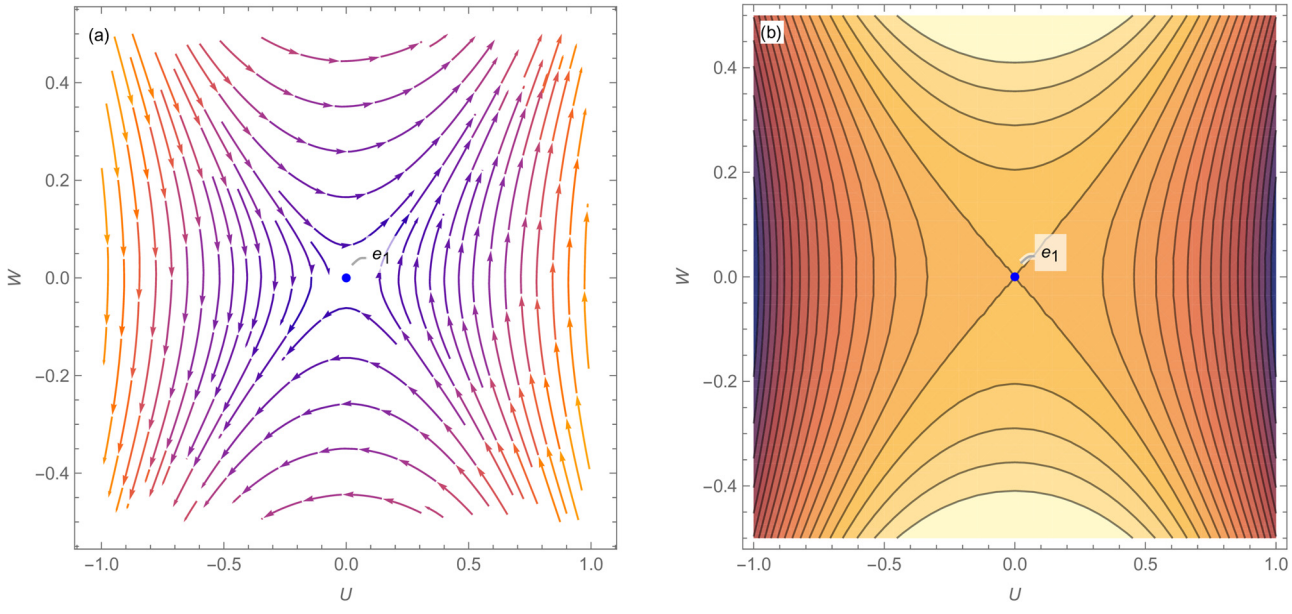

Figure 14: (a) Phase plot and (b) Contour plot of system (35) with parameters: $\mathcal{A}_1 = 3$, $\mathcal{A}_2 = 1$, and $\mathcal{A}_3 = -2$.

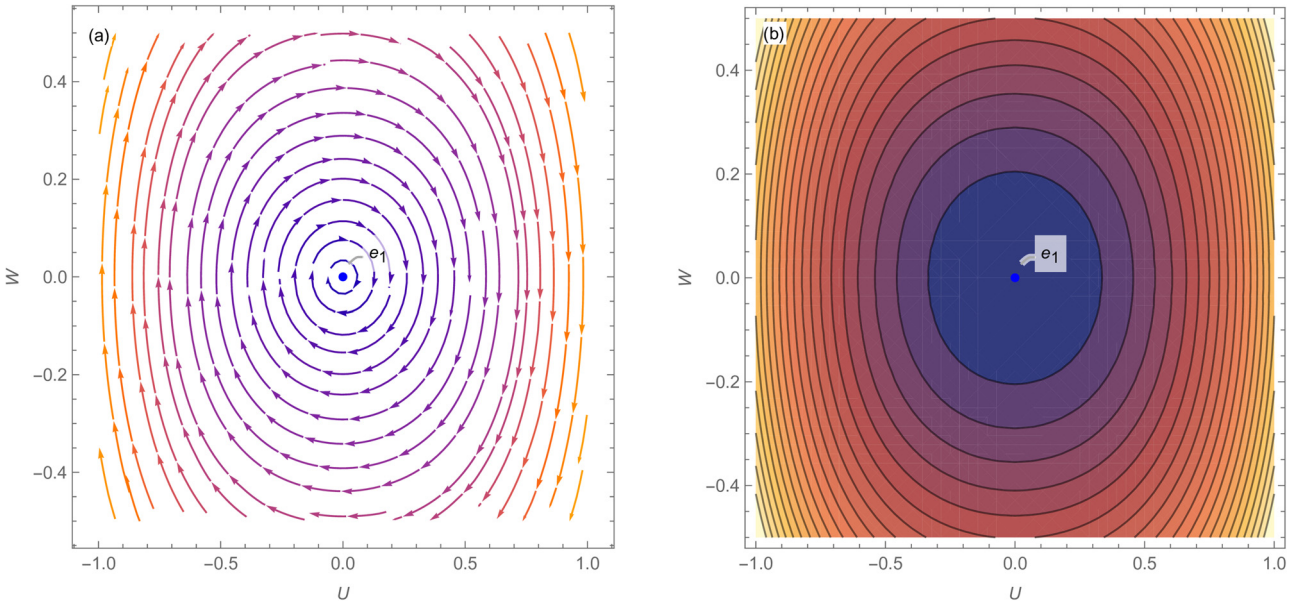

Figure 15: (a) Phase plot and (b) Contour plot of system (35) with parameters: $\mathcal{A}_1 = -3$, $\mathcal{A}_2 = 1$, and $\mathcal{A}_3 = -2$.

$$H(U, W) = \frac{W^2}{2} + \frac{1}{4\mathcal{A}_1}(\mathcal{A}_3U^4 - 2\mathcal{A}_2U^2) = h. \quad (36)$$

The dynamical system (35) with parameters $\mathcal{A}_1, \mathcal{A}_2, \mathcal{A}_3$ in the $UW-$ phase plane has three equilibrium points $e_i = (U_i, W)$, $i = 1, 2, 3$, where $U_1 = 0$, $U_2 = \sqrt{\frac{\mathcal{A}_2}{\mathcal{A}_3}}$, $U_3 = -\sqrt{\frac{\mathcal{A}_2}{\mathcal{A}_3}}$ and $W = 0$. We determine the Jacobian matrix determinant of system (35)

$$\mathcal{D}_i = |J(U_i, W)| = \frac{1}{\mathcal{A}_1}(3U_i^2\mathcal{A}_3 - \mathcal{A}_2), \quad i = 1, 2, 3. \quad (37)$$

Now, we display four cases for the bifurcation of phase portraits as follows:

Case 1: If $\mathcal{A}_2\mathcal{A}_3 < 0$ and $\mathcal{A}_1\mathcal{A}_2 > 0$, there exist one equilibrium point $e_1(0,0)$ of system (35) and $\mathcal{D}_{e_1(0,0)} < 0$, that is a saddle point that has homoclinic orbits as shown in Figure 14.

Case 2: If $\mathcal{A}_2\mathcal{A}_3 < 0$ and $\mathcal{A}_1\mathcal{A}_2 < 0$, obtain one equilibrium point $e_1(0,0)$ of system (35), and $\mathcal{D}_{e_1(0,0)} > 0$ that is a center point that has periodic orbits (Figure 15).

Case 3: If $\mathcal{A}_2\mathcal{A}_3 > 0$ and $\mathcal{A}_1\mathcal{A}_2 > 0$, obtain three equilibrium points of system (35) as follows: (i) The saddle point $e_1(0,0)$, has $\mathcal{D}_{e_1(0,0)} < 0$, (ii) the center points $e_2(\sqrt{\frac{\mathcal{A}_2}{\mathcal{A}_3}}, 0)$ and $e_3(-\sqrt{\frac{\mathcal{A}_2}{\mathcal{A}_3}}, 0)$ have positive signs of the Jacobian $\mathcal{D}_{2,3}$ corresponding to $e_2(\sqrt{\frac{\mathcal{A}_2}{\mathcal{A}_3}}, 0)$ and $e_3(-\sqrt{\frac{\mathcal{A}_2}{\mathcal{A}_3}}, 0)$, respectively. Consequently, Figure 17 shows that the trajectories of the equilibrium points that are superperiodic orbits.

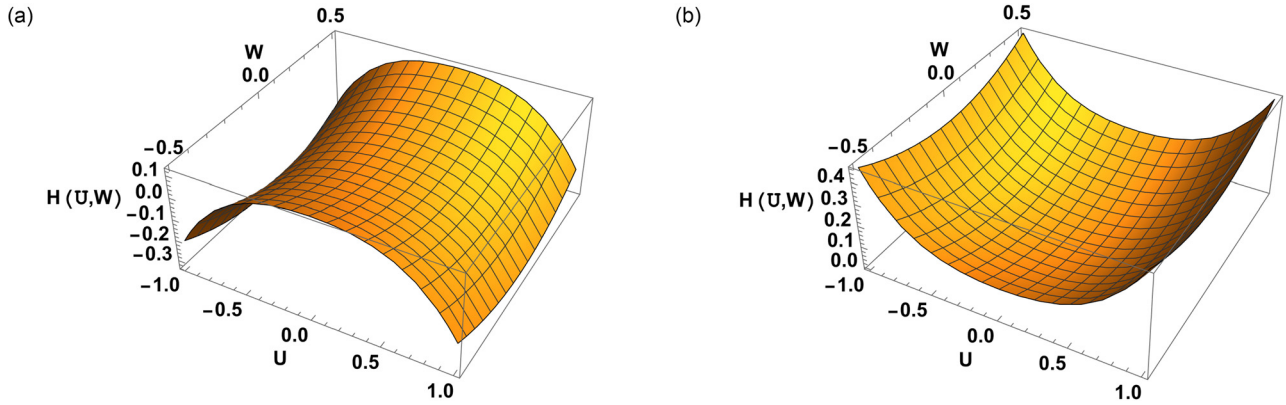

Figure 16: 3D plots of (36): (a) $\mathcal{A}_1 = 3$, $\mathcal{A}_2 = 1$, $\mathcal{A}_3 = -2$ and (b) $\mathcal{A}_1 = -3$, $\mathcal{A}_2 = 1$, $\mathcal{A}_3 = -2$.

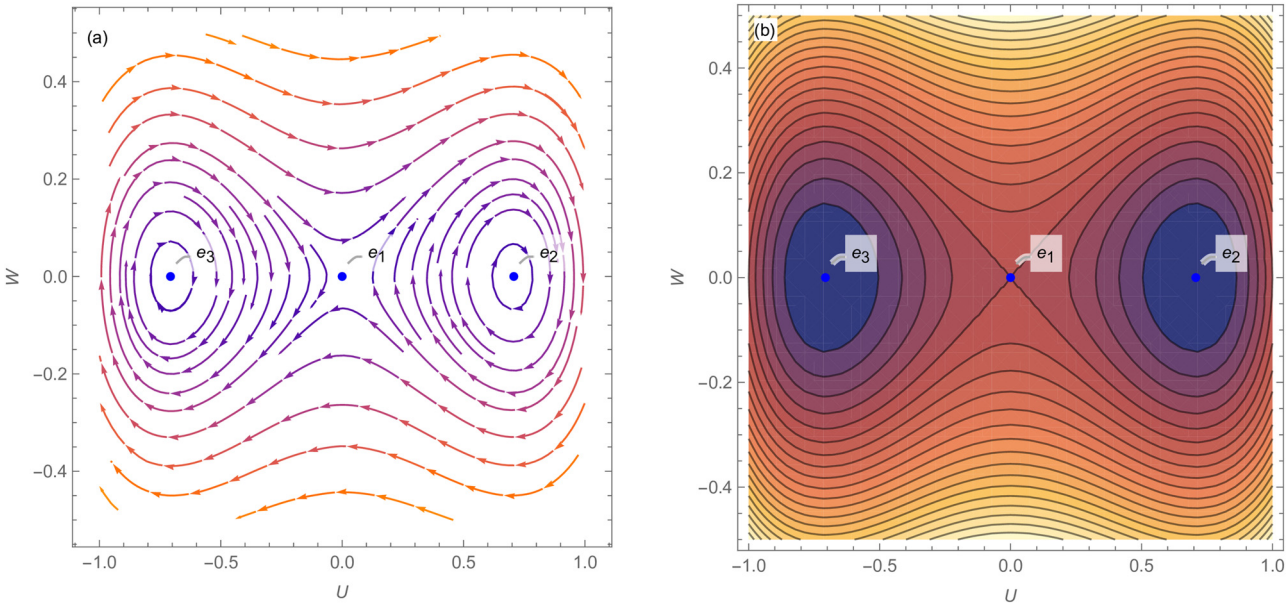

Figure 17: (a) Phase plot and (b) Contour plot of system (35) with parameters: $\mathcal{A}_1 = 3$, $\mathcal{A}_2 = 1$, $\mathcal{A}_3 = 2$.

Case 4: If $\mathcal{A}_2\mathcal{A}_3 > 0$ and $\mathcal{A}_1\mathcal{A}_2 < 0$, acquire three equilibrium points of system (35) as follows: (i) the center point $e_1(0,0)$, has $\mathcal{D}_{e_1(0,0)} > 0$, (ii) the saddle points $e_2(\sqrt{\frac{\mathcal{A}_2}{\mathcal{A}_3}}, 0)$ and $e_3(-\sqrt{\frac{\mathcal{A}_2}{\mathcal{A}_3}}, 0)$, have negative signs of the Jacobian $\mathcal{D}_{2,3}$ matching $e_2(\sqrt{\frac{\mathcal{A}_2}{\mathcal{A}_3}}, 0)$ and $e_3(-\sqrt{\frac{\mathcal{A}_2}{\mathcal{A}_3}}, 0)$, respectively. So, Figure 18 exhibits the trajectories of the equilibrium points that are hetroclinic orbits. Then, all phase portraits and contour plots of system (35) are shown in 2D plots (Figures 14–18). While Figures 16 and 19 exhibit 3D plots of the total energy defined by the Hamiltonian function (36).

8 Chaotic analysis

In this section, we illustrate the chaotic behaviors of the dynamical system presented in (35). This study is offered for three cases of this system, the first for unexcited system, the second for excited system by a parametric

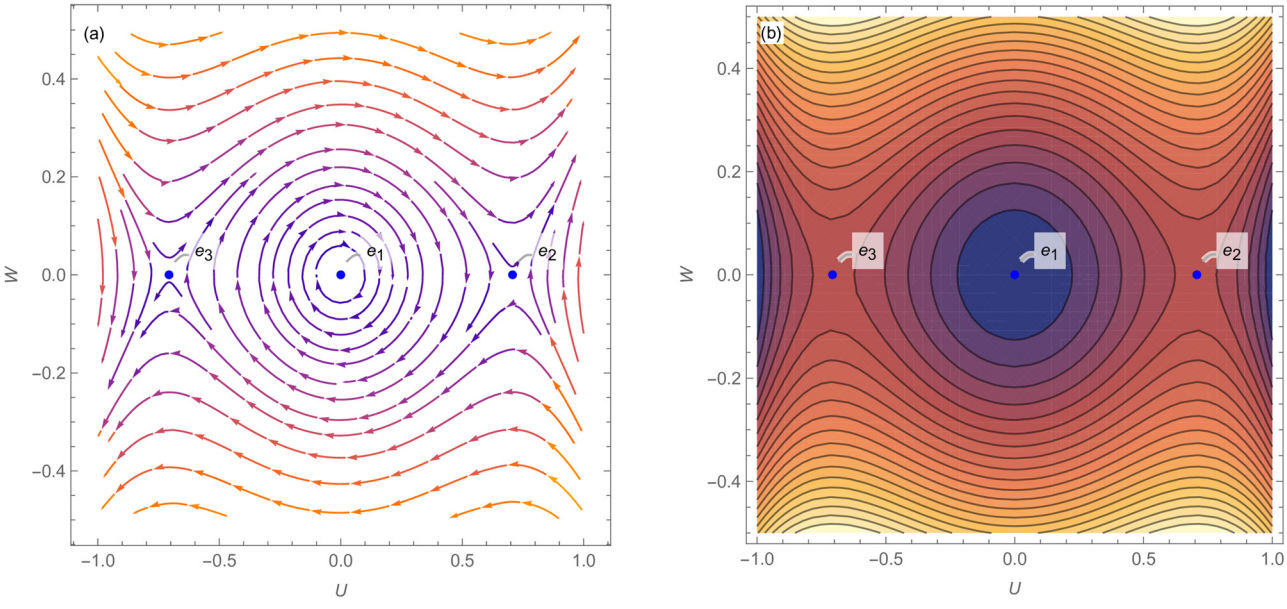

Figure 18: (a) Phase plot and (b) Contour plot of system (35) with parameters: $\mathcal{A}_1 = -3$, $\mathcal{A}_2 = 1$, $\mathcal{A}_3 = 2$.

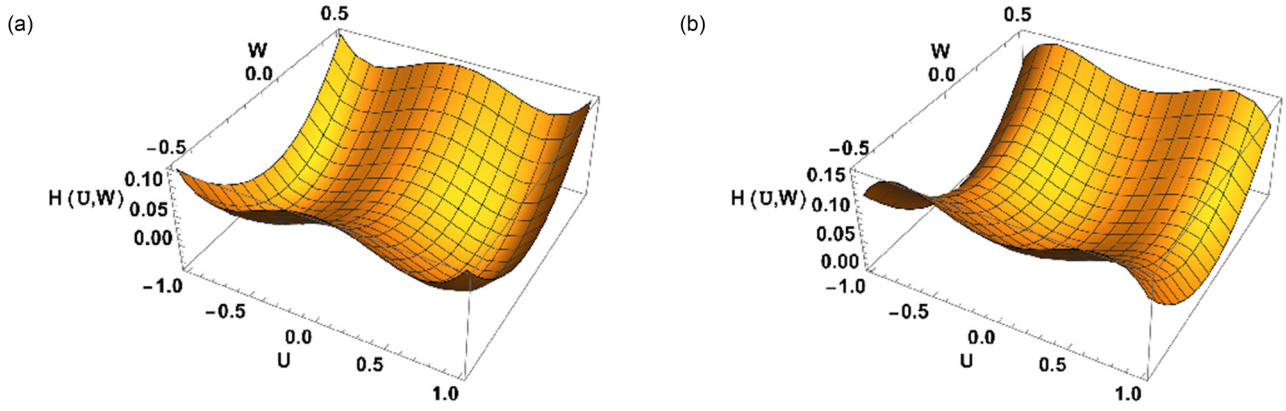

Figure 19: 3D plots of (36): (a) $\mathcal{A}_1 = 3$, $\mathcal{A}_2 = 1$, $\mathcal{A}_3 = 2$ and (b) $\mathcal{A}_1 = -3$, $\mathcal{A}_2 = 1$, $\mathcal{A}_3 = 2$.

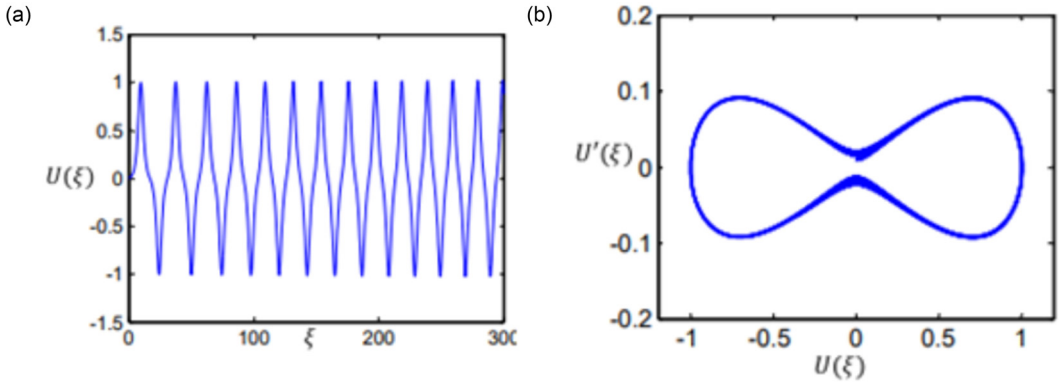

Figure 20: (a) Time history and (b) Poincare mapping of unexcited system (35) with parameters: $\mathcal{A}_1 = 3$, $\mathcal{A}_2 = 1$, and $\mathcal{A}_3 = 2$.

excitation force, and the third for control excited system using proportional feedback control (P-Controller).

8.1 Chaotic behaviors for unexcited system

We use time histories and Poincare mapping to investigate the chaotic behaviors for unexcited system (35). Figures 20 and 21 present time histories and Poincare mapping of unexcited system for the cases, $\mathcal{A}_1\mathcal{A}_2 > 0$, $\mathcal{A}_3\mathcal{A}_2 > 0$, and $\mathcal{A}_1\mathcal{A}_2 < 0$, $\mathcal{A}_3\mathcal{A}_2 < 0$. From these figures, we can conclude that system (35) is stable as shown in time histories in Figures 20(a) and 21(a). Also, system (35) is quasi-periodic as shown by Poincare mapping in Figures 20(b) and 21(b).

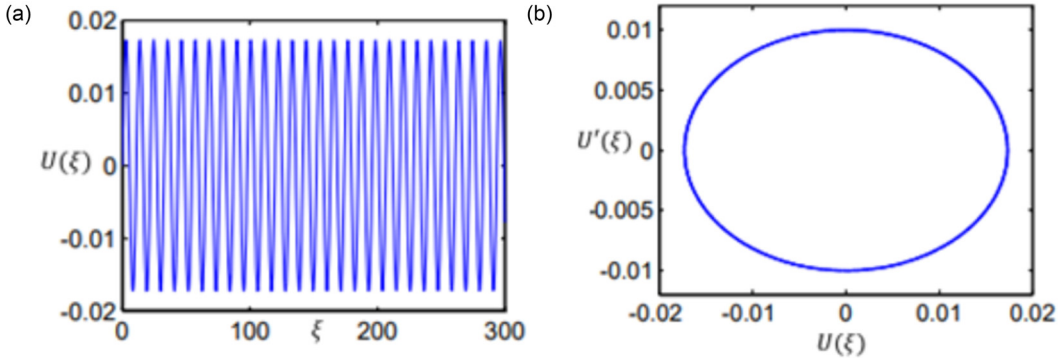

Figure 21: (a) Time history and (b) Poincare mapping of unexcited system (35) with parameters: $\mathcal{A}_1 = 3$, $\mathcal{A}_2 = -1$, and $\mathcal{A}_3 = 2$.

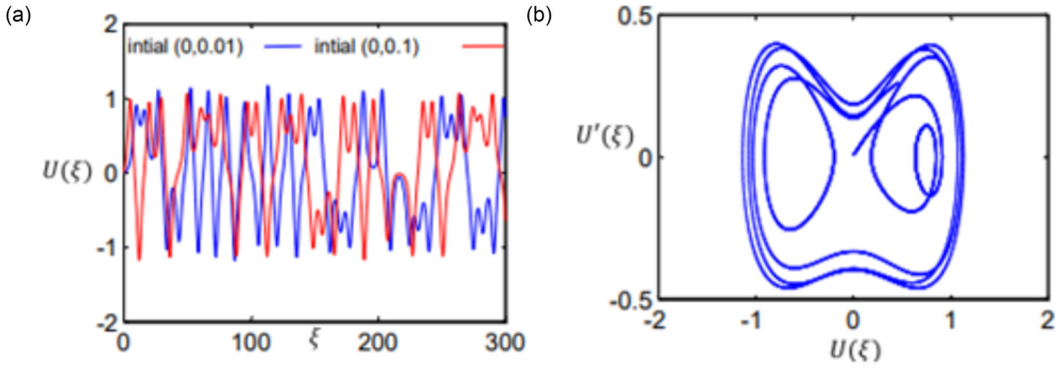

Figure 22: (a) Time history and (b) Poincare mapping of excited system (38) with parameters: $\mathcal{A}_1 = 3$, $\mathcal{A}_2 = -1$, $\mathcal{A}_3 = 2$, $f = 0.1$, and $\chi = 0.5$.

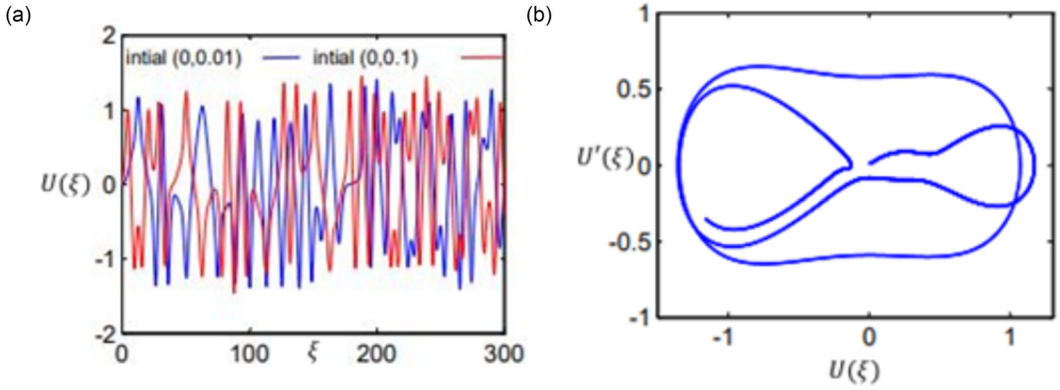

Figure 23: (a) Time history and (b) Poincare mapping of excited system (38) with parameters: $\mathcal{A}_1 = 3$, $\mathcal{A}_2 = -1$, $\mathcal{A}_3 = 2$, $f = 0.3$, and $\chi = 0.5$.

8.2 Chaotic behaviors for excited system

We modulated the dynamical system presented in (35) by adding a parametric excitation force as follows:

$$\begin{aligned} U'(\xi) &= W(\xi), \\ W'(\xi) &= \frac{\mathcal{A}_2}{\mathcal{A}_1}(U(\xi)) - \frac{\mathcal{A}_3}{\mathcal{A}_1}(U(\xi))^3 + fU(\xi)\cos(\chi\xi), \end{aligned} \tag{38}$$

where f and χ are the amplitude and the frequency of the parametric force, respectively. We investigated the periodic behavior of the excited dynamical system presented in (38) using time histories and Poincare mapping, as shown in Figures 22–24. These figures show the influence of the parametric excitation force on the system which made the system unstable and chaotic. Moreover, the parametric force effects on sensitivity to the initial conditions of

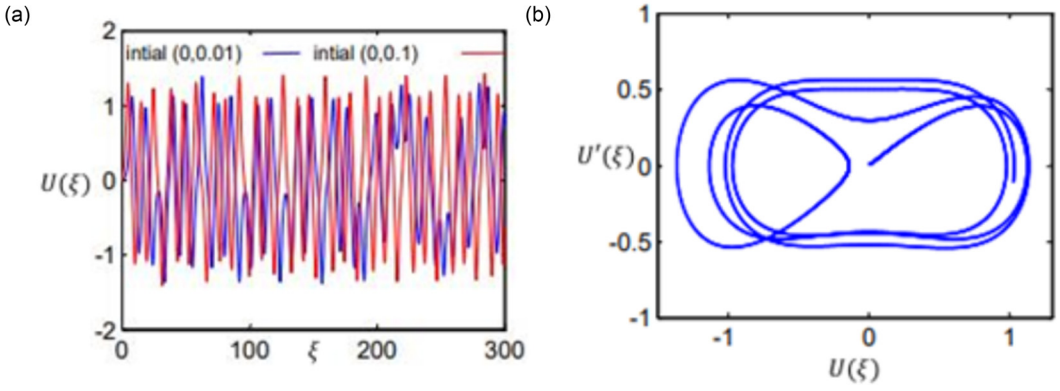

Figure 24: (a) Time history and (b) Poincare mapping of excited system (38) with parameters: $\mathcal{A}_1 = 3$, $\mathcal{A}_2 = -1$, $\mathcal{A}_3 = 2$, $f = 0.3$, and $\chi = 0.2$.

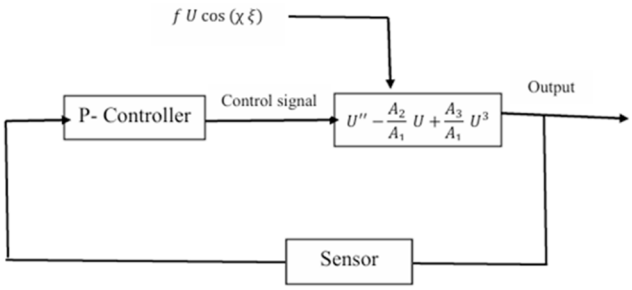

Figure 25: Closed loop of controlled system (39).

the dynamical system. Therefore, this system must be controlled using a different type of control.

8.3 Chaotic behaviors for control excited system

To suppress the vibrations of the dynamical system presented in (38), we will use the proportional feedback control (P-Controller) to improve system stability. P-Controller can be represented mathematically by $F(\xi) = -kU(\xi)$, where $F(\xi)$ is the output of the proportional controller, $U(\xi)$ is the error signal, and k is the proportional gain parameter as shown in the block diagram in Figure 25. So, the system presented in (38) after using P-Controller takes the form:

$$\begin{aligned} U'(\xi) &= W(\xi), \\ W'(\xi) &= \frac{\mathcal{A}_2}{\mathcal{A}_1}(U(\xi)) - \frac{\mathcal{A}_3}{\mathcal{A}_1}(U(\xi))^3 + fU(\xi)\cos(\chi\xi) \\ &\quad + F(\xi). \end{aligned} \tag{39}$$

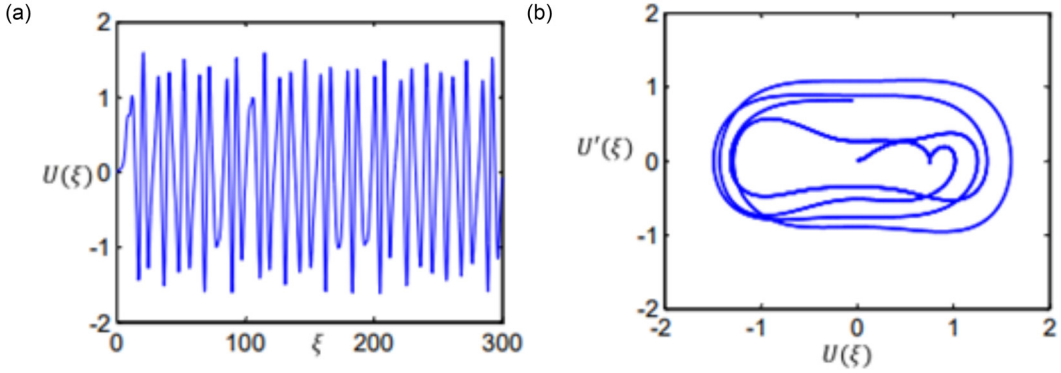

Figure 26: (a) Time history and (b) Poincare mapping of excited system (39) with parameters: $\mathcal{A}_1 = 3$, $\mathcal{A}_2 = 1$, $\mathcal{A}_3 = 2$, $f = 0.3$, $\chi = 1.2$, and $k = 0$.

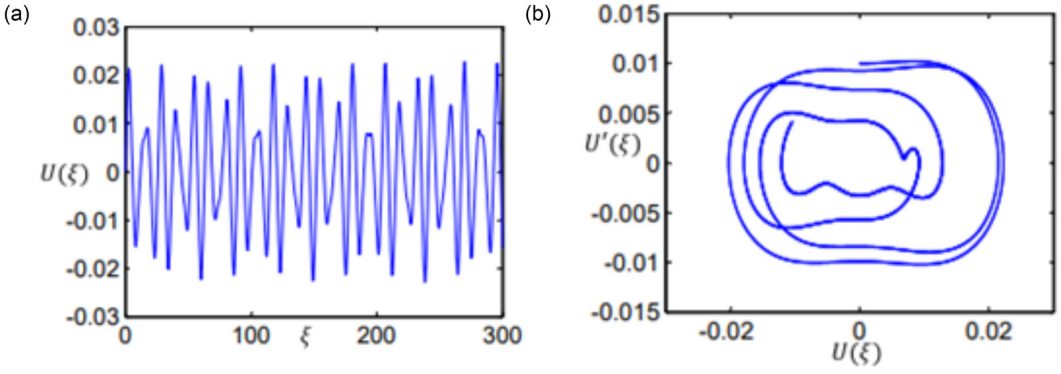

Figure 27: (a) Time history and (b) Poincare mapping of excited system (39) with parameters: $\mathcal{A}_1 = 3$, $\mathcal{A}_2 = 1$, $\mathcal{A}_3 = 2$, $f = 0.3$, $\chi = 1.2$, and $k = 0.5$.

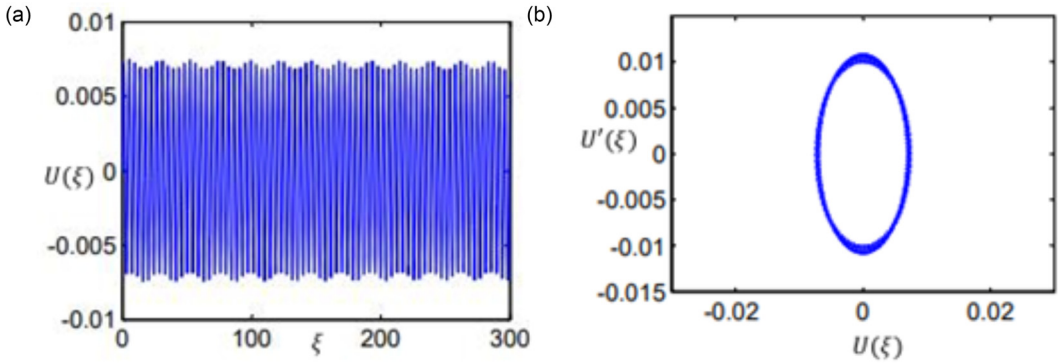

Figure 28: (a) Time history and (b) Poincare mapping of excited system (39) with parameters: $\mathcal{A}_1 = 3$, $\mathcal{A}_2 = 1$, $\mathcal{A}_3 = 2$, $f = 0.3$, $\chi = 1.2$, and $k = 2.5$.

We study the controlled system (39) with the following values of parameters: $\mathcal{A}_1 = 3$, $\mathcal{A}_2 = 1$, $\mathcal{A}_3\mathcal{A}_2 = 2$, $f = 0.3$, $\chi = 1.2$, and different values of the proportional gain parameter. For $k = 0$ (P-Controller deactivated), the dynamical system (39) has high amplitude and still unstable with chaotic behavior as presented in Figure 26. When the P-Controller activated the amplitude of the dynamical system (39) decreased as shown in Figures 27 and 28. In Figure 27, we take $k = 0.5$; so, the amplitude decreases to 0.02, which means that the effectiveness of P-Controller $\left(E_{\mathrm{a}} = \frac{\text{amplitude without controller}}{\text{amplitude with controller}}\right)$ equals 60 but the system will still be unstable and chaotic. In Figure 28, by increasing the value of k to 2.5, the amplitude decreases to 0.007, which means that $E_{\mathrm{a}} = 171$ and system (39) becomes stable with limit cycle phase.

9 Conclusion

In this study, we have explored the optical soliton solutions and bifurcation analysis of the Sasa–Satsuma equation, emphasizing its chaotic behaviors and modulation instability within nonlinear optical systems. Utilizing the $(\mathcal{H} + \frac{\mathcal{G}'}{\mathcal{G}^2})$-expansion method, we derived analytical solutions that illustrate the complex dynamics of solitons in optical fibers. Our analysis of modulation instability revealed the critical role of higher-order nonlinear effects, which can significantly influence the stability of optical signals. We conducted a thorough bifurcation analysis, employing time histories and Poincaré mapping to investigate the chaotic behaviors induced by parametric excitation. Additionally, we implemented a proportional feedback control (P-Controller) to manage the vibrations of the dynamical system effectively. The graphical representations provided in both 2D and 3D formats enhance our understanding of the soliton solutions and their behaviors under various conditions. Overall, our findings contribute valuable insights into the dynamics of NPDEs, with implications for advancements in nonlinear optics and related fields. Future work may focus on further exploring these phenomena under different parameters and conditions, as well as applying the methodologies to other nonlinear systems.

Acknowledgments: The authors extend their appreciation to Taif University, Saudi Arabia, for supporting this work through project number (TU-DSPP-2024-73).

Funding information: The authors extend their appreciation to Taif University, Saudi Arabia, for supporting this work through project number (TU-DSPP-2024-73).

Author contributions: All authors have accepted responsibility for the entire content of this manuscript and approved its submission.

Conflict of interest: The authors state no conflict of interest.

Data availability statement: Data sharing is not applicable to this article as no data sets were generated or analyzed during the current study.

References

[1] Ablowitz M, Prinari B, Trubatch AD. Discrete and continuous nonlinear Schrödinger systems. Cambridge: Cambridge University Press; 2004.

[2] Hong WP. Optical solitary wave solutions for the higher order nonlinear Schrödinger equation with cubic-quintic non-Kerr terms. Opt Commun. 2001;194:217–23.

[3] Ismael1 HF, Sulaiman TA, Osman MS. Multi-solutions with specific geometrical wave structures to a nonlinear evolution equation in

the presence of the linear superposition principle. Commun Theoret Phys. 2022;75:1.
[4] Malik S, Almusawa H, Kumar S, Wazwaz A, Osman MS. A (2+1)-dimensional Kadomtsev-Petviashvili equation with competing dispersion effect: Painlevé analysis, dynamical behavior and invariant solutions. Results Phys. 2021;23:104043.
[5] Biswas A, Milovic D. Bright and dark solitons of the generalized nonlinear Schrödingers equation. Commun Nonlinear Sci Numer Simul. 2010;15:1473–84.
[6] L"u X, Lin F, Qi F. Analytical study on a two-dimensional Korteweg'de Vries model with bilinear representation, Bäcklund transformation and soliton solutions. Appl Math Model. 2015;39(12):3221–6.
[7] Yao S, Ullah N, Rehman HU, Hashemi MS, Mirzazadeh M, Inc M. Dynamics on novel wave structures of non-linear Schrödinger equation via extended hyperbolic function method. Results Phys. 2023;48:106448.
[8] Islam SMR, Akbulut A, Arafat SMY. Exact solutions of the different dimensional CBS equations in mathematical physics. Partial Differ Equ Appl Math. 2022;5:100320.
[9] BiswasA, MilovicD, KohlR. Optical soliton perturbation in a log-law medium with full non linearity by He's semi-inverse variational principle. Inverse Probl Sci Eng. 2012;20(2):227–32.
[10] BiswasA. 1-soliton solution of the generalized Radhakrishnan, Kundu, Lakshmanan equation. Phys Lett A. 2009;373:2546–48.
[11] Constantin P. Chicago Lectures in Mathematics Series. University of Chicago; 1988.
[12] Attia RAM, Lu D, Khater MMA. Structure of new solitary solutions for the Schwarzian Korteweg De Vries equation and (2 + 1)-Ablowitz-Kaup-Newell-Segur equation. Phys J. 2018;1:2581–7396.
[13] VendhanCP. A study of Berger equations applied to non-linear vibrations of elastic plates, Int J Mech Sci. 1975;17:461–8.
[14] Iqbal MA, Gepreel KA, Ali Akbar M and Osman MS. The compatibility and dynamics of optical soliton solutions for higher-order nonlinear Schrödinger model. Mod Phys Lett. B. 2024;39(22):2550086.
[15] Ur Rehman H, Jafar S, Javed A, Hussain S, and Tahir M. New optical solitons of Biswas-Arshed equation using different techniques. Optik. 2020;206:163670.
[16] Tahir M, Awan AU, Ur Rehman H. Optical solitons to Kundu-Eckhaus equation in birefringent fibers without four-wave mixing. Optik. 2019;199:163297.
[17] Ur Rehman H, Said GS, Amer A, Ashraf H, Tharwat MM, Abdel-Aty M, et al. Unraveling the (4+1)-dimensional Davey-Stewartson-Kadomtsev-Petviashvil equation: Exploring soliton solutions via multiple techniques. Alexandr Eng J. 2024;90:17–23.
[18] Xu T, Wang D, Li M, Liang H. Soliton and breather solutions of the Sasa-Satsuma equation via the Darboux transformation. Phys Scr. 2014;7:89.
[19] Akram G, Sadaf M, Arshed S, Sabir H. Optical soliton solutions of fractional Sasa-Satsuma equation with beta and conformable derivatives. Opt Quantum Electron. 2022;54:741.
[20] Hosseini K, Sadri K, Salahshour S, Baleanu D, Mirzazadeh M, Inc M. The generalized Sasa-Satsuma equation and its optical solitons. Opt Quantum Electron. 2022;54:723.
[21] Li C, Chen L, Li G. Optical solitons of space-time fractional Sasa-Satsuma equation by F-expansion method. Optik. 2020;224:165527.
[22] Yildirim Y. Optical solitons to Sasa-Satsuma model with modified simple equation approach. Optik. 2019;184:271–6.
[23] Samir I, Ahmed H, Mirzazadeh M, Triki H. Derivation new solitons and other solutions for higher order Sasa-Satsuma equation by using the improved modified extended tanh scheme. Optik. 2023;274:170592.
[24] Hosseini K, Mirzazadeh M, Gömez-Aguilar JF. Soliton solutions of the Sasa-Satsuma equation in the mono mode optical fibers including the beta-derivatives. Optik. 2020;224:165425.
[25] Li Z, Xie X, Jin C. Optical solitons to the coupled cubic-quartic Sasa-Satsuma equation with Kerr law nonlinearity in birefringent fibers. Optik. 2022;269:169886.
[26] Kuang Y, Zhu J. The higher-order soliton solutions for the coupled Sasa-Satsuma system via the ∂-dressing method. Appl Math Lett. 2017;66:47–53.
[27] Kuang Y, Mao B, Wang X. Higher-order soliton solutions for the Sasa-Satsuma equation revisited via ∂ method. J Nonl Math Phys. 2023;30:1821–33.
[28] Demiray ST, Pandir Y, Bulut H. New soliton solutions for Sasa-Satsuma equation. Waves Random Complex Media. 2015;25:1–12.
[29] Khater MMA, Seadawy AR, Lu D. Dispersive optical soliton solutions for higher order nonlinear Sasa-Satsuma equation in mono mode fibers via new auxiliary equation method. Superlattice Microst. 2018;113:346–58.
[30] Wazwaz A, Mehanna M. Higher-order Sasa-Satsuma equation: Bright and dark optical solitons. Optik. 2021;243, 167421.
[31] Shakeel M, Ali Shah N, Dong Chung J. Novel analytical technique to find closed form solutions of time fractional partial differential equations. Fractal Fract. 2022;6:1–22.
[32] Shaikh TS, Baber MZ, Ahmed N, Iqbal MS, Akgül A, El Din SM. Acoustic wave structures for the confirmable time-fractional Westervelt equation in ultrasound imaging. Results Phys. 2023;49:106494.
[33] Baber MZ, Rezazadeh H, Iqbal MS, Ahmed N, Yasin MW, Hosseinzadeh MA. Investigation of soliton solutions for the NWHS model with temperature distribution in an infinitely long and thin rod. Modern Phys Lett B. 2024;18:2450392.
[34] Zakharov VE, Ostrovsky LA. Modulation instability: The beginning. Phys D Nonl Phenomena. 2009;5:540–8.
[35] Tanemura T, Ozeki Y, Kikuchi K. Modulational instability and parametric amplification induced by loss dispersion in optical fibers. Phys Rev Lett. 2004;93:163902.
[36] Akinyemi L, Houwe A, Abbagari S, Wazwaz A, Alshehri HM, Osman MS Effects of the higher-order dispersion on solitary waves and modulation instability in a monomode fiber. Optik. 2023;288:171202.
[37] Guckenheimer J, Holmes PJ. Nonlinear oscillations, dynamical systems and bifurcations of vector fields. New York: Springer; 1983.
[38] Hosseini K, Hinçal E, Alizadeh F, Baleanu D, Osman MS. Bifurcation analysis, sensitivity analysis, and Jacobi Elliptic function structures to a generalized nonlinear Schrödinger equation. Int J Theor Phys. 2024;63:306.
[39] Gu Y, Peng L, Huang Z, Lai Y. Soliton, breather, lump, interaction solutions and chaotic behavior for the (2+1)-dimensional KPSKR equation. Chaos Solitons Fractals. 2024;187:115351.
[40] Gu Y, Zhang X, Huang L, Peng L, Lai Y, Aminakbari N. Soliton and lump and travelling wave solutions of the (3 + 1) dimensional KPB like equation with analysis of chaotic behaviors. Sci Rep. 2024;14:20966.
[41] Gu Y, Jiang C, Lai Y. Analytical solutions of the fractional Hirota-Satsuma coupled KdV equation along with analysis of bifurcation, sensitivity and chaotic behaviors. Fract Fract. 2024;8(10):585.
[42] Atepor L, Akoto RNA. Dynamic effect of the parametric excitation force on an autoparametric vibration absorber. Russian J Nonl Dyn. 2022;18(1):137–57.
[43] Amer YA, Abd EL-Salam MN, EL-Sayed MA. Behavior of a hybrid Rayleigh-Van der Pol-duffing oscillator with a PD controller. J Appl Res Tech. 2022;20(1):58–67.